



1 **Parameterizations of US wildfire and prescribed fire emission**
2 **ratios and emission factors based on FIREX-AQ aircraft**
3 **measurements**

4 Georgios I. Gkatzelis ^{1,2,†}, Matthew M. Coggon ², Chelsea E. Stockwell ^{1,2}, Rebecca S. Hornbrook ³,
5 Hannah Allen ⁴, Eric C. Apel ³, Katherine Ball ⁴, Megan M. Bela ^{1,2}, Donald R. Blake ⁵, Ilann Bourgeois
6 ^{1,2}, Steven S. Brown ^{2,6}, Pedro Campuzano-Jost ^{1,6}, Jason M. St. Clair ^{7,8}, James H. Crawford ⁹, John D.
7 Crouse ¹⁰, Douglas A. Day ^{1,6}, Joshua P. DiGangi ⁹, Glenn S. Diskin ⁹, Alan Fried ¹¹, Jessica B. Gilman
8 ², Hongyu Guo ^{1,6}, Johnathan W. Hair ⁹, Hannah S. Halliday ^{9,‡}, Thomas F. Hanisco ⁷, Reem Hannun ⁷,
9 ¹², Alan Hills ³, L. Gregory Huey ¹³, Jose L. Jimenez ^{1,6}, Joseph M. Katich ^{1,2}, Aaron Lamplugh ^{1,2},
10 Young Ro Lee ¹³, Jin Liao ^{7,14}, Jakob Lindaas ^{15,§}, Stuart A. McKeen ^{1,2}, Tomas Mikoviny ¹⁶, Benjamin
11 A. Nault ^{1,6,||}, J. Andrew Neuman ^{1,2}, John B. Nowak ⁹, Demetrios Pagonis ^{1,6,¶}, Jeff Peischl ^{1,2}, Anne
12 E. Perring ^{1,17}, Felix Piel ^{16,18,19}, Pamela S. Rickly ^{1,2}, Michael A. Robinson ^{1,2,6}, Andrew W. Rollins ²,
13 Thomas B. Ryerson ^{2,^}, Melinda K. Schueneman ^{1,6}, Rebecca H. Schwantes ², Joshua P. Schwarz ²,
14 Kanako Sekimoto ²⁰, Vanessa Selimovic ²¹, Taylor Shingler ⁹, David J. Tanner ¹³, Laura Tomsche ^{9,22,*},
15 [#], Krystal T. Vasquez ¹⁰, Patrick R. Veres ², Rebecca Washenfelder ², Petter Weibring ¹⁰, Paul O.
16 Wennberg ^{10,23}, Armin Wisthaler ^{16,18}, Glenn M. Wolfe ⁷, Caroline C. Womack ^{1,2}, Lu Xu ^{10,+}, Robert J.
17 Yokelson ²¹, Carsten Warneke ²

18
19 ¹ Cooperative Institute for Research in Environmental Sciences, University of Colorado Boulder, Boulder, CO,
20 USA

21 ² NOAA Chemical Sciences Laboratory (CSL), Boulder, CO, USA

22 ³ Atmospheric Chemistry Observations & Modeling Laboratory, NCAR, Boulder, CO, USA

23 ⁴ Division of Chemistry and Chemical Engineering, California Institute of Technology, Pasadena, CA, USA

24 ⁵ Department of Chemistry, University of California, Irvine, CA, USA

25 ⁶ Department of Chemistry, University of Colorado Boulder, Boulder, CO, USA

26 ⁷ Atmospheric Chemistry and Dynamics Laboratory, NASA Goddard Space Flight Center, Greenbelt, MD, USA

27 ⁸ Joint Center for Earth Systems Technology, University of Maryland Baltimore County, Baltimore, MD, USA

28 ⁹ NASA Langley Research Center, Hampton, VA, USA

29 ¹⁰ Division of Geological and Planetary Sciences, California Institute of Technology, Pasadena, CA, USA

30 ¹¹ Institute of Arctic & Alpine Research, University of Colorado, Boulder, CO, USA

31 ¹² Joint Center for Earth Systems Technology, University of Maryland Baltimore County, Baltimore, MD, USA

32 ¹³ School of Earth and Atmospheric Sciences, Georgia Institute of Technology, Atlanta, GA, USA

33 ¹⁴ Universities Space Research Association, Columbia, MD, USA

34 ¹⁵ Colorado State University, Department of Atmospheric Science, Fort Collins, CO, USA

35 ¹⁶ Department of Chemistry, University of Oslo, Oslo, Norway

36 ¹⁷ Department of Chemistry, Colgate University, Hamilton, NY, USA

37 ¹⁸ Institut für Ionenphysik und Angewandte Physik, Universität Innsbruck, Innsbruck, Austria

38 ¹⁹ IONICON Analytik GmbH, Innsbruck, Austria

39 ²⁰ Graduate School of Nanobioscience, Yokohama City University, 22-2 Seto, Kanazawa-ku, Yokohama,
40 Kanagawa, Japan

41 ²¹ Department of Chemistry and Biochemistry, University of Montana, Missoula, MT, USA

42 ²² Universities Space Research Association, Columbia, MD, USA

43 ²³ Division of Engineering and Applied Science, California Institute of Technology, Pasadena, CA, USA

44 Currently at:

45 [†] Institute of Energy and Climate Research, IEK-8: Troposphere, Forschungszentrum Jülich GmbH, Jülich,
46 Germany

47 [‡] U.S. Environmental Protection Agency, Research Triangle Park, NC, USA

48 [§] AGI / AAAS Congressional Science Fellow

49 ^{||} Center for Aerosol and Cloud Chemistry, Aerodyne Research Inc., Billerica, MA, USA

50 [¶] Weber State University, Ogden, UT, USA

51 [^] Scientific Aviation, Boulder, CO, USA

52 ^{*} Institute of Atmospheric Physics, German Aerospace Center, Weßling, Germany



53 #Johannes Gutenberg University, Mainz, Germany

54 + Cooperative Institute for Research in Environmental Sciences, University of Colorado Boulder, Boulder, CO,

55 USA and NOAA Chemical Sciences Laboratory (CSL), Boulder, CO, USA

56 *Correspondence to:* (g.gkatzelis@juelich.de and matthew.m.coggon@noaa.gov)

57 **Abstract.**

58 Extensive airborne measurements of non-methane organic gases (NMOGs), methane, nitrogen oxides, reduced
59 nitrogen-species, and aerosol emissions from US wild and prescribed fires were conducted during the 2019
60 NOAA/NASA Fire Influence on Regional to Global Environments and Air Quality campaign (FIREX-AQ). Here,
61 we report the atmospheric enhancement ratios (ERs) and inferred emission factors (EFs) for compounds measured
62 onboard the NASA DC-8 research aircraft for nine wildfires and one prescribed fire, which encompass a range of
63 vegetation types.

64 We use photochemical proxies to identify young smoke and reduce the effects of chemical degradation on our
65 emissions calculations. ERs and EFs calculated from FIREX-AQ observations agree within a factor of 2 with values
66 reported from previous laboratory and field studies for more than 80% of the carbon- and nitrogen-containing
67 species. Wildfire emissions are parameterized based on correlations of the sum of NMOGs with reactive nitrogen
68 oxides (NO_y) to modified combustion efficiency (MCE) as well as other chemical signatures indicative of
69 flaming/smoldering combustion, including carbon monoxide (CO), nitrogen dioxide (NO_2), and black carbon
70 aerosol. The sum of primary NMOG EFs correlates to MCE with an R^2 of 0.68 and a slope of $-296 \pm 51 \text{ g kg}^{-1}$,
71 consistent with previous studies. The sum of the NMOG mixing ratios correlates well with CO with an R^2 of 0.98
72 and a slope of $137 \pm 4 \text{ ppbv}$ of NMOGs per ppmv of CO, demonstrating that primary NMOG emissions can be
73 estimated from CO. Individual nitrogen-containing species correlate better with NO_2 , NO_y , and black carbon than
74 with CO. More than half of the NO_y in fresh plumes is NO_2 with an R^2 of 0.95 and a ratio of NO_2 to NO_y of $0.55 \pm$
75 $0.05 \text{ ppbv ppbv}^{-1}$, highlighting that fast photochemistry had already occurred in the sampled fire plumes. The ratio
76 of NO_y to the sum of NMOGs follows trends observed in laboratory experiments and increases exponentially with
77 MCE, due to increased emission of key nitrogen species and reduced emission of NMOGs at higher MCE during
78 flaming combustion. These parameterizations will provide more accurate boundary conditions for modeling and
79 satellite studies of fire plume chemistry and evolution to predict the downwind formation of secondary pollutants,
80 including ozone and secondary organic aerosol.



81 **1 Introduction**

82 Open biomass burning in the form of wildfires, prescribed forest management fires, and agricultural burns is one of
83 the largest sources of trace gases and aerosols worldwide (Akagi et al., 2011; Crutzen and Andreae, 1990). It is the
84 dominant global source of black carbon and primary organic aerosol (Bond et al., 2013), and accounts for more than
85 20% of the global emissions of nitric oxide (NO) and carbon monoxide (CO) (Olivier et al., 2005; Yokelson et al.,
86 2008; Wiedinmyer et al., 2011). It is the second largest global source of non-methane organic gases (NMOGs)
87 (Akagi et al., 2011), and a major source of greenhouse gases, including methane (CH₄), carbon dioxide (CO₂), and
88 nitrous oxide (N₂O) that impact the atmospheric carbon budget and climate (Sudo and Akimoto, 2007; Ward et al.,
89 2012; Tian et al., 2016; Le Quéré et al., 2018).

90 During the last decade, the number of wildfires and prescribed fires in the US has sometimes exceeded 74,000 and
91 450,000 yr⁻¹, respectively (National Interagency Fire Center). Warming temperatures, drier climate, and a history of
92 fire suppression are projected to increase the frequency and intensity of wildfires and lengthen fire seasons globally
93 (Spracklen et al., 2009; Kloster et al., 2010; Pechony and Shindell, 2010; Moritz et al., 2012; Flannigan et al., 2013;
94 Mann et al., 2016; Balch et al., 2017), which is already evident in the western US, Canada, the eastern Mediterranean,
95 Siberia, and Australia (Westerling et al., 2006; Keywood et al., 2013; Yue et al., 2015). Wildfires in the US largely
96 occur in the western conterminous states and Alaska, and typically account for 12 to 40 thousand km² of the annual
97 total area burned (National Interagency Fire Center). In the southeastern US, prescribed fires and agricultural burns
98 are a common land management tool used to improve ecosystem health or facilitate planting crops (Wiedinmyer
99 and Hurteau, 2010; Cochrane et al., 2012). Since prescribed fires in the southeast currently account for about 25
100 thousand km² per year on average (National Interagency Fire Center), it is also important to characterize their
101 emissions.

102 While wildfires and prescribed fires are favorable for many ecosystem functions, the atmospheric impacts of fire on
103 climate, air quality, and health are a major concern. Particles directly emitted or formed via chemical processes have
104 direct and indirect effects on climate by influencing the regional and global radiation balance and impacting cloud
105 properties and precipitation (Braga et al., 2017; Cecchini et al., 2017; Hamilton et al., 2018; Thornhill et al., 2018;
106 Kodros et al., 2020). Global mortality from outdoor pollution due to biomass burning smoke accounts for 600,000
107 premature deaths per year (Johnston et al., 2012), with particulate matter (PM) and O₃ posing the greatest risk factors
108 (Akagi et al., 2014; Dennekamp et al., 2015; Brey and Fischer, 2015; Knorr et al., 2017; Apte et al., 2018). In smoke
109 plumes, O₃ and secondary organic aerosols are photochemically produced from the interplay of NO_x, NMOGs, and
110 meteorology (Tsimpidi et al., 2017; Hodshire et al., 2019). An essential first step to elucidate the factors contributing
111 to PM and O₃ pollution downwind fires is to quantify primary gas- and particle-phase emissions.

112 Numerous studies have quantified emission factors (EFs; grams emitted per kg of dry fuel burned) for various fuel
113 types and different fire characteristics using ground-based or airborne measurements in close proximity to
114 wildland/prescribed fire plumes (e.g., Stockwell et al., 2016; Liu et al., 2017; Peng et al., 2020; Mouat et al., 2021;
115 Lindaas et al., 2021; Permar et al., 2021) or controlled laboratory burns (e.g., Stockwell et al., 2014; Koss et al.,
116 2018; Selimovic et al., 2018). Literature reviews to combine these results have been periodically conducted (Andreae
117 and Merlet, 2001; Akagi et al., 2011; Andreae, 2019), with the most recent by Prichard et al. (2020). Nevertheless,
118 uncertainties in the process-level understanding and model representation of fire emissions, plume rise, and
119 chemistry still exist, which influence model performance in accurately capturing downwind O₃ and secondary
120 organic aerosol formation (Müller et al., 2016; Reddington et al., 2016; Shrivastava et al., 2017). These uncertainties
121 can result from an insufficient understanding of the chemistry and total emissions of NO_x and NMOGs across fuel
122 types, ecosystems, and fire combustion conditions (Warneke et al., 2011; Yokelson et al., 2013; Hatch et al., 2017).

123 In this study, we calculate western US wildfire emission factors for a broad range of gas- and particle-phase species
124 measured aboard the NASA DC-8 during the 2019 Fire Influence on Regional to Global Environments and Air
125 Quality (FIREX-AQ) campaign, which included the most comprehensive payload to date for airborne sampling of
126 biomass burning emissions. We compare our results to the most recent laboratory and airborne field studies,
127 including the fire sciences laboratory component of FIREX-AQ (hereafter referred to as FireLab) (Koss et al., 2018),
128 the fourth Fire Lab at Missoula Experiment, FLAME-4 (Stockwell et al., 2015), the Western Wildfire Experiment
129 for Cloud Chemistry, Aerosol Absorption, and Nitrogen, WE-CAN (Permar et al., 2021), and the Studies of

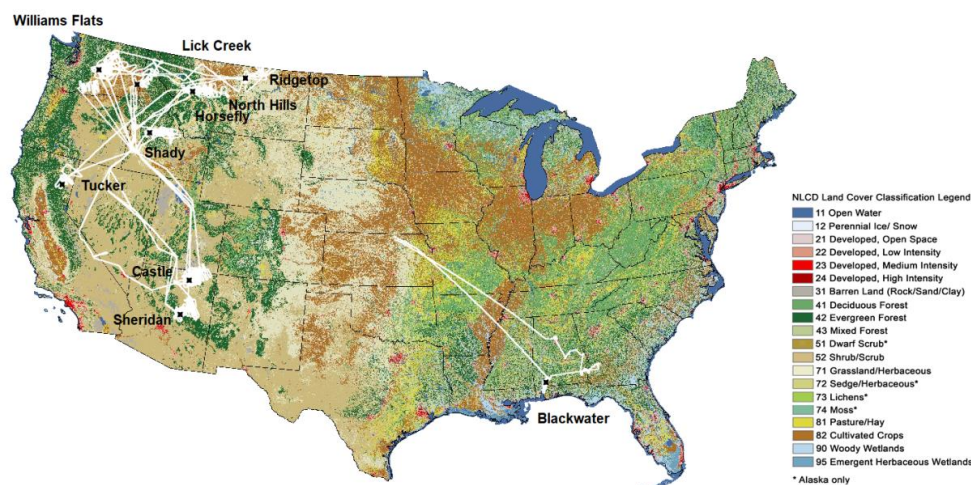


130 Emissions and Atmospheric Composition, Clouds and Climate Coupling by Regional Surveys, SEAC⁴RS (Liu et
 131 al., 2017; Wolfe et al., 2022), as well as results summarised in the review by Andreae (2019). We parameterize
 132 wildfire emissions based on correlations of carbon- and nitrogen-containing species to CO, NO₂, black carbon, and
 133 modified combustion efficiency (MCE) to improve future modeling efforts to accurately capture the chemical
 134 evolution of wildfire smoke.

135 2 Methods

136 2.1 Platforms and Instrumentation

137 The NASA DC-8 aircraft was deployed with an extensive suite of instruments to measure the gas- and particle-
 138 phase pollutants emitted and photochemically produced downwind of US wildfires. Figure 1 and Table 1 show the
 139 research flights analyzed here to capture freshly emitted wildfire smoke from 22 July to 3 September 2019. In total,
 140 16 crosswind plume transects downwind from 9 western wildfires and 1 eastern prescribed fire are analyzed, which
 141 represent a range of fuel types, including timber, grass, dead trees, logging debris, brush, and litter. The transects
 142 are selected based on aging proxies to examine emissions with minimal atmospheric processing. The physical age
 143 is determined based on transect proximity to the fire, an estimated plume rise time, and wind speed (Holmes et al.,
 144 2020) and ranged from 10–153 min (1–40 km) downwind for the plumes described here. The MCE, defined as
 145 $\Delta\text{CO}_2/(\Delta\text{CO}_2+\Delta\text{CO})$, is commonly reported to quantify the fire conditions and describes the relative amount of
 146 flaming and smoldering combustion (Yokelson et al., 1996). Pure flaming fires have an MCE near 0.99, while
 147 smoldering fires vary over a wider range but are most often near 0.8 (Akagi et al., 2011). For the freshest plume
 148 crossings, the MCE was on average 0.90 ± 0.04 (range 0.94–0.85), suggesting a mix of flaming and smoldering
 149 emissions.



150

151 **Figure 1:** Selected NASA DC-8 flight tracks for sampling the wildfire and prescribed fire plumes during the 2019 FIREX-AQ.
 152 Fires discussed in this study are denoted by black markers. The US map is colored by land cover classification according to the
 153 2019 National Land Cover Database (<https://www.mrlc.gov/>).

154 Multiple instruments performed fast response *in situ* measurements of gas- and particle-phase species summarized
 155 in Table 2. The University of Colorado aircraft aerosol mass spectrometer (CU HRAMS, AMS in the following)
 156 (Canagaratna et al., 2007; Guo et al., 2021) measured organic aerosol, particulate ammonium, and nitrate (pNO_y)
 157 that consisted of inorganic nitrates (pNO₃), organic nitrates (pRONO₂), and nitroaromatics (pArNO₂) (Day et al.,
 158 2022). Black carbon aerosol concentration was measured by a Single-Particle Soot Photometer (SP2) and scaled
 159 (~10%) to represent the total accumulation-mode (Schwarz et al., 2008). NMOGs were measured by the NOAA
 160 proton transfer reaction time-of-flight mass spectrometer (PTR-ToF-MS) (Yuan et al., 2016), two whole-air



161 samplers, namely the NOAA integrated Whole Air Sampler (NOAA iWAS) (Lerner et al., 2017) and the University
 162 of California, Irvine Whole Air Sampler (UCI WAS) (Colman et al., 2001; Simpson et al., 2020), the NCAR Trace

163 **Table 1:** Freshest plume crossings identified for analysis during FIREX-AQ 2019.

Fire	Transect number	Date and Time, UTC	Fuel Type	Maleic anhydride to furan as an indicator of OH exposure (ppb ppb ⁻¹)	Physical age (s)	MCE
Shady	0	7/25/2019 22:48	Understory: Ponderosa pine, white-Douglas fir, quaking aspen, two-needle pinyon-Utah juniper forest w/ open shrubs, grasses, and timber litter	0.09	1350	0.91
Shady	9	7/25/2019 23:47		0.07	1250	0.90
North Hills	0	7/29/2019 23:21	Savanna: Ponderosa pine savanna, Douglas-fir-Pacific ponderosa pine, ocean spray forest with Idaho fescue-bluebunch wheatgrass	0.13	600	0.86
Tucker	0	7/30/2019 2:40	Shrubland: Sagebrush-greasewood shrubland with open grasses	0.12	1720	0.91
Ridgetop	4	8/2/2019 23:18	Grassland: Bluebunch wheatgrass, bluegrass with sagebrush-greasewood shrubs and savanna	0.14	2620	0.94
Lick Creek	1	8/3/2019 1:13	Forest: Grand-Douglas fir, Pacific ponderosa pine, ocean spray forest	0.15	1500	0.91
Williams Flats	0	8/3/2019 22:22	Grassland: Idaho fescue-bluebunch wheatgrass-cheatgrass, sagebrush shrublands under open Douglas-fir-Pacific ponderosa pine, ocean spray savanna/forest	0.16	890	0.91
Williams Flats	21	8/4/2019 0:41		0.14	6130	0.91
Horsefly	1	8/6/2019 23:20	Forest: Managed: Subalpine-Douglas fir, lodgepole-whitebark-Pacific ponderosa-Mature lodgepole pine, Engelmann spruce oceanspray forest	0.12	3890	0.87
Horsefly	3	8/6/2019 23:28		0.11	6250	0.85
Williams Flats	7	8/9/2019 1:49	Forest: Douglas-fir-Pacific ponderosa pine, ocean spray forest with grassland understory	0.11	5460	0.91
Castle	0	8/13/2019 0:18	Forest: Ponderosa pine, two-needle-pinyon-Utah juniper, Douglas-white fir, Madrean pine-oak, quaking aspen forest	0.15	1540	0.90
Castle	0	8/13/2019 23:17		0.16	9200	0.90
Castle	10	8/14/2019 1:32		0.07	1600	0.88
Sheridan	1	8/17/2019 0:42	Forest: Pinyon-Utah juniper forest with Turbinella oak-alderleaf mountain mahogany shrubland	0.15	1200	0.91
Blackwater	8	8/30/2019 17:11	Forest: Prescription, primarily shrubs, grasses and litter from loblolly-longleaf-slash pine, willow-laurel-turkey-water oak, and magnolia forest	0.31	580	0.93

164 **Table 2:** Descriptions of the instrumentation aboard the NASA DC-8 used in this study.

Species Measured	Technique	Frequency [Hz]	Inlet Setup	Reference
O ₃ , NO, NO ₂ , NO _y	Chemiluminescence	1	PFA, approx. 1 m long, 1 slpm for each species; NO and NO ₂ additionally pass through 50.9 cm ³ quartz cells	Ryerson et al. (2000)



CO ₂ , CO, CH ₄ , H ₂ O	2x Laser Absorption Spectroscopy	1-5	¼ in stainless steel, 2 m long, 3slpm flow	<i>Sachse et al. (1991)</i> <i>Bourgeois et al. (2022)</i>
NH ₃ , speciated hydrocarbons and OVOCs	PTR-ToF-MS	1 (NH ₃) 10 (others)	PFA, 2 m long, ~20 LPM (before Aug 3), ~60 LPM (from Aug 3 onwards), heated to 60°C	<i>Müller et al. (2016)</i> <i>(with modifications)</i>
PAN, PPN, other PANs	Chemical Ionization Mass Spectrometry (CIMS)	1-10	½" FEP tubing	<i>Zheng et al. (2011)</i>
HONO, HCN, HNCO, HCOOH, N ₂ O ₅ , HPMTF, halogenated compounds	Iodide ToF-CIMS	1	PTFE, 1m long, 6 SLPM, heated to 40°C	<i>Veres et al. (2020)</i>
NO	Laser Induced Fluorescence	1	PFA and silcosteel, 1m length, unheated, overflow at 10-20 slm	<i>Rollins et al. (2020)</i>
CH ₂ O, C ₂ H ₆	Laser Absorption Spectroscopy	1	Heated HIAPER inlet followed by several meters of heated PTFE Teflon tubing	<i>Richter et al. (2015);</i> <i>Fried et al. (2020)</i>
C ₂ -C ₁₀ Alkanes, C ₂ -C ₄ Alkenes, C ₆ -C ₉ Aromatics, C ₁ -C ₅ Alkyl nitrates, etc.	Whole Air Sampling	Up to 168 per flight	stainless steel	<i>Simpson et al. (2001)</i>
Speciated hydrocarbons and OVOCs	H ₃ O ⁺ ToF-CIMS	1-5	PTFE, 1m long, 1-2 LPM, heated to 50°C	<i>Yuan et al. (2016)</i>
C ₂ -C ₁₀ Alkanes, C ₂ -C ₄ Alkenes, C ₆ -C ₉ Aromatics, C ₁ -C ₅ Alkyl nitrates, etc.	Whole Air Sampling	Up to 72 per flight	PFA, 2m Long, ~60 LPM, unheated	<i>Lerner et al. (2017)</i>
C ₃ -C ₁₀ hydrocarbons, C ₁ -C ₇ OVOCs, HCN, CH ₃ CN, halogenated VOCs, etc.	HR-ToF-GC/MS	0.0095	Restek Silcosteel, 2.5 LPM, heated to 40°C	<i>Apel et al. (2010)</i>
CH ₂ O	Laser Induced Fluorescence	1-10	PFA and silcosteel, 1m length, unheated, overflow at 10-20 slm	<i>Cazorla et al. (2015)</i>
H ₂ O ₂ , organic peroxides, organic acids, isoprene oxidation products, etc.	CIMS	1	A glass tube (3 cm ID and 47cm long) coated with a thin layer of (Fluoropel PFC 801A, Cytonix Corp.). The tube is gently heated and the sampling flow rate through the glass tube is >=40 m/s.	<i>Crouse et al. (2006)</i>
glyoxal, methylglyoxal, HONO, NO ₂	Airborne Cavity Enhanced Spectrometer	1	PTFE teflon, <1 m length, inlet heated to 25°C, 10.5 vlpn	<i>Min et al. (2016)</i>
BC mass concentration	SP2	1	NASA Langley inlet with optional dilution	<i>Schwarz et al. (2008)</i>
Submicron aerosol composition	CU-HR-AMS	1 (up to 10 Hz in plumes)	HIMIL tall inlet, 1.3 m SS 0.18" ID+ 0.45 m 0.08" ID tubing + pressure controlled instrument inlet (<0.3 s total residence time)	<i>Guo et al (2021);</i> <i>Canagaratna et al (2007)</i>

165 Organic Gas Analyzer (Apel et al., 2015), a fast online gas chromatograph outfitted with a Time-of-Flight mass
 166 spectrometer (TOGA-TOF), the Caltech chemical ionization time-of-flight mass spectrometer (CIT-ToF-CIMS),
 167 and for selected flights the University of Innsbruck / University of Oslo (UIBK/UiO) PTR-ToF-MS (prototype PTR-
 168 TOF 4000X2; IONICON Analytik GmbH, Innsbruck, Austria). Three instruments were used in this study that
 169 measured formaldehyde: the In Situ Airborne Formaldehyde (ISAF) instrument (Liao et al., 2021), the Compact
 170 Atmospheric Multispecies Spectrometer (CAMS) (Weibring et al., 2007), and the UIBK/UiO PTR-ToF-MS. ISAF
 171 and CAMS correlated with an R² coefficient of 0.99 and a slope of 1.27, as discussed by Liao et al. (2021); whereas



172 the UIBK/UiO PTR-ToF-MS agreed better with the CAMS, with a slope of 1.02. In this study, we use the ISAF
173 measurements, which have the best time response compared to all other instruments and adjust the mixing ratios to
174 match those reported by CAMS and the UIBK/UiO PTR-ToF-MS. The NOAA Iodide ion chemical ionization mass
175 spectrometer (NOAA CIMS) (Veres et al., 2020) was used to measure formic acid (HCOOH), nitrous acid (HONO),
176 and dinitrogen pentoxide (N₂O₅). CO and CH₄ were measured via mid-IR wavelength modulation spectroscopy by
177 the Differential Absorption Carbon Monoxide Measurement (DACOM) instrument (Sachse et al., 1991). CO₂ was
178 measured via nondispersive infrared absorption spectroscopy using a LICOR model 7000 analyzer (Vay et al, 2009).
179 NO, NO₂, and NO_y were measured by the NOAA chemiluminescence instrument (Bourgeois et al., 2020). NO_y
180 measures the sum of reactive nitrogen compounds, including NO, NO₂, HONO, peroxy nitrates, alkyl and
181 multifunctional nitrates, and particulate nitrate. Additional measurements of HONO and NO₂ were provided by the
182 NOAA Airborne Cavity Enhanced Spectrometer (ACES) (Min et al., 2016) and NO by the NOAA Laser Induced
183 Fluorescence instrument (NO-LIF) (Rollins et al., 2020). Glyoxal and methylglyoxal were measured by ACES, and
184 ammonia (NH₃) by the UIBK/UiO PTR-ToF-MS (Müller et al., 2016; Tomsche et al., 2023). The Georgia Tech
185 CIMS (GT-CIMS) was used to measure peroxyacetyl nitrate (PAN) and other PAN-like compounds such as
186 peroxypropionyl nitrate, peroxyacryloyl nitrate, and peroxybutyryl nitrate. Finally, the plume structure was
187 obtained from aerosol backscatter measured with the NASA Langley Airborne Differential Absorption Lidar
188 (DIAL). All measurements reported here are provided in the NASA FIREX-AQ data repository (NASA airborne
189 science data for atmospheric composition, 2019).

190 In this study, we focus on quantifying total and speciated NMOG emissions, which were predominantly measured
191 by PTR-ToF-MS, the two Whole Air Samplers, and TOGA-TOF. The same NOAA PTR-ToF-MS and the iWAS
192 systems were used at the US Forest Service's Missoula Fire Sciences Laboratory (FireLab) in 2016 as a precursor
193 to FIREX-AQ and described by Koss et al. (2018). Koss et al. (2018) speciated isomers measured by PTR-ToF-MS
194 using gas chromatography pre-separation and reported isomer distributions for over 150 individual masses. Here,
195 we compare these isomer distributions to the speciation derived based on the comparison of the GC-MS and PTR-
196 ToF-MS measurements conducted aboard the NASA DC-8 (Table S5). Two calibration methods were used to
197 determine NMOG sensitivities for the PTR-ToF-MS. For commercially available compounds, sensitivities were
198 determined by gravimetrically prepared standards or by liquid calibration, as described by Coggon et al. (2019).
199 Sensitivities for other species were estimated based on calculated proton transfer rate coefficients, as described by
200 Sekimoto et al. (2017). For the WAS system(s), NMOGs were calibrated using gravimetrically prepared standards,
201 as described by Lerner et al. (2017). A detailed description of the PTR-ToF-MS and WAS setups as well as NMOG
202 uncertainty is included in the supplement.

203 **3 Results and discussion**

204 **3.1 Plumes with minimal photochemical aging**

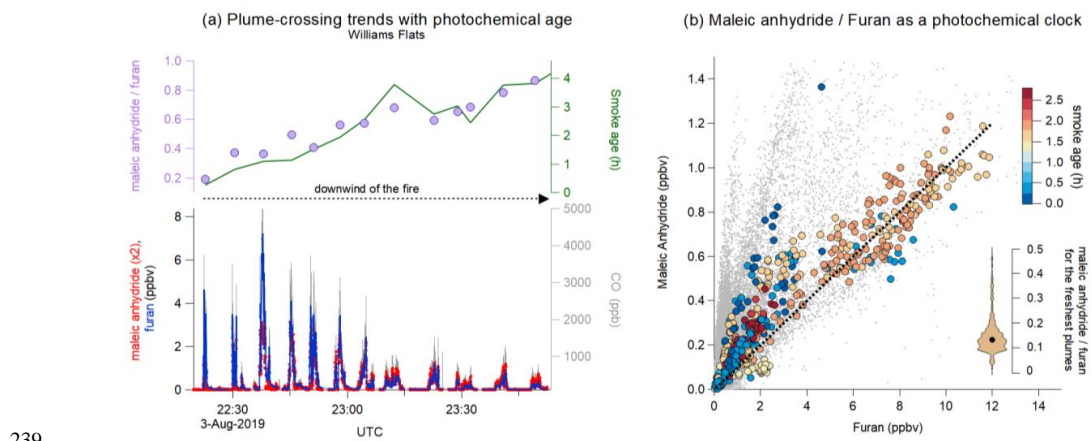
205 Emissions from wildfire plumes chemically transform once injected into the atmosphere (e.g., Akagi 2012;
206 Robinson et al., 2021; Decker et al., 2021; Xu et al., 2021). However, safety and operational constraints limit the
207 proximity of airborne sampling to the fire. An essential first step to quantifying wildfire primary emissions is to
208 identify plume samples that have undergone minimal chemical processing. Commonly, the freshest plumes are
209 identified using the plume age calculated from the distance downwind of the wildfire using the onboard measured
210 average wind speed (e.g., Permar et al., 2021) but neglecting plume rise. The physical age does not necessarily
211 identify plume crossings with the least chemical processing since the sampled smoke can be impacted by
212 meteorology, solar radiation, radical concentrations, and sampling artifacts related to the aircraft's position relative
213 to the center of the plume (Robinson et al., 2021; Decker et al., 2021; Wang et al., 2021).

214 Here, we account for oxidation by hydroxyl radical (OH) using the ratio of primary and secondary NMOG wildfire
215 tracers, specifically furan (a primary species; Koss et al., 2018) and maleic anhydride (a slow-reacting, secondary
216 species observed downwind of fires) (Zhao and Wang, 2017). Coggon et al. (2019) show that maleic anhydride
217 quickly forms downwind of fires from the OH oxidation of furans, and Wang et al. (2021) show that the distribution
218 of maleic anhydride in plumes closely mirrors the distribution of OH exposure. Since furan is a direct wildfire
219 emission and maleic anhydride is a chemical product of furan chemistry that is not significantly emitted from fires
220 (Coggon et al., 2019; Wang et al., 2021), the ratio of maleic anhydride to furan (MA/F) is expected to increase



221 downwind of a fire and exhibit a minimum in the least-processed plumes. This ratio is used as a photochemical
 222 clock to identify the freshest sampled plumes by extracting the lowest MA/F transect per wildfire plume and reduce
 223 the effects of chemical degradation on our primary NMOG emission calculations. We note that this technique may
 224 not account for the faster photolysis of light-absorbing species (such as HONO) or fast interconversion between NO
 225 and NO₂, but that the sum of reactive nitrogen species (NO_y) is expected to be conserved downwind of fires (Lindaas
 226 et al., 2020). Also, a quantitative relationship between MA/F and OH exposure is not presented here as the yield of
 227 maleic anhydride from furan oxidation requires further laboratory quantification.

228 Figure 2a shows the maleic anhydride, furan, and CO concentration downwind of the Williams Flats wildfire on
 229 August 3, 2019, as a characteristic example. Also shown are the MA/F and the median physical smoke age calculated
 230 for each plume crossing. Here we use the high time resolution of PTR-ToF-MS for MA and furan concentrations,
 231 but furan is additionally scaled by 0.46 to match the TOGA GC-MS concentrations as discussed in Sect. 3.2. VOC
 232 and CO concentrations were highest closer to the wildfire and decreased downwind, primarily due to dilution. The
 233 MA/F increased from 0.20 to 0.86 downwind of the fire, indicating active chemical conversion of furan to maleic
 234 anhydride. The physical smoke age followed the same increase from 0.5 to 4 hours. Figure 2b shows the MA/F for
 235 all wildfire plumes and the extracted freshest plume crossings. The freshest plume crossings had a median MA/F of
 236 0.13 (0.1–0.16, 25th–75th), and their corresponding physical age was less than 1.46 h (0.6–1.74) (see Table 1).
 237 However, certain fires with similar MA/F ratios drastically ranged in physical age from 15 minutes to as high as 3–
 238 4 hours.



239

240 **Figure 2:** (a) Mixing ratios of maleic anhydride, furan, and CO (bottom) and ratios of maleic anhydride to furan (top) in 12
 241 crosswind plume transects of smoke from the Williams Flats fire on 3 August 2019. The maleic anhydride to furan ratio increases
 242 as the plume ages during transport away from the Williams Flats. (b) Comparison of the maleic anhydride and furan mixing
 243 ratios used as a photochemical clock to identify the freshest plume crossings during FIREX-AQ. Grey points are all 1-sec
 244 resolution measurements during FIREX-AQ, and circles are the chosen freshest plume crossings colored by the physical smoke
 245 age. The violin plot shows the variability of the ratio of maleic anhydride to furan for the freshest wildfire transects.

246 Figure S1 further highlights differences in the physical and chemical age of a fire by focusing on the Williams Flats
 247 wildfire and the Blackwater prescribed fire. The DIAL image shows the shape and evolution of the wildfire smoke
 248 from overpass flights. For the Williams Flats fire, the DC-8 sampled emissions by performing raster patterns
 249 perpendicular to the smoke, whereas for the Blackwater fire, the DC-8 also flew along the smoke plume at various
 250 altitudes. For the Blackwater fire, the MA/F increased rapidly up to 1.4 ppbv ppbv⁻¹ 30 km downwind of the wildfire,
 251 while for the Williams Flats fire, the ratio reached a maximum of 1 ppbv ppbv⁻¹ 120 km downwind of the fire. These
 252 differences highlight the importance of accounting for the chemical rather than the physical age of a fire to determine
 253 the freshest transects. The MA/F for fresh, unaged smoke during the FireLab study was ~ 0.04 ppbv ppbv⁻¹ (Wang
 254 et al., 2021), showing that even the freshest plume transects sampled during FIREX-AQ were partially
 255 photochemically processed, with a median MA/F that was 0.14 ppbv ppbv⁻¹. Fire plumes sampled closest to the
 256 emission source that showed significant chemical processing with a MA/F > 0.20 are excluded from this analysis.



257 The exception is the Blackwater prescribed fire that was the only fire representative of southeastern US fuel types
258 included in our analysis, even though the freshest plume crossing had a MA/F of 0.3. Further evaluation of biases
259 during FIREX-AQ for fast-reacting species is discussed in Sect. 3.3.

260 3.2 Instrument comparisons

261 NMOG measurements obtained from the NOAA PTR-ToF-MS were compared to other instruments onboard the
262 DC-8, including TOGA-TOF, 2 WAS systems, CIT-CIMS, UIBK/UiO PTR-ToF-MS, and NOAA CIMS. Table S5
263 provides correlations of the PTR-ToF-MS measurements to other instruments. For calibrated compounds, the
264 NOAA PTR-ToF-MS and the UIBK/UiO PTR-ToF-MS agreed within 10–35% for methanol, acetonitrile, acetone,
265 methyl ethyl ketone (MEK), benzene, toluene, C₈ and C₉ aromatics, and monoterpenes. The NOAA PTR-ToF-MS,
266 and NOAA CIMS agreed within uncertainty for hydrogen cyanide (HCN), isocyanic acid (HNCO), and formic acid,
267 respectively. CIT-CIMS agreed with the NOAA PTR-ToF-MS for HCN whereas for phenol it was lower by a factor
268 2. Both instruments were calibrated for phenol suggesting that differences could be due to PTR-ToF-MS
269 fragmentation of higher molecular weight gases that produce signals at the phenol ion mass, or differences in the
270 detection of other isomers from the two instruments.

271 Although the PTR-ToF-MS provides high time resolution measurements, it cannot speciate NMOG isomers detected
272 at the same exact mass. In the following, we compare mixing ratios derived for the PTR-ToF-MS chemical formula
273 to the combined isomer signals derived from GC-MS, given in parentheses. When compared to the iWAS, WAS,
274 and TOGA-TOF measurements, the NOAA PTR-ToF-MS was within ±25–35% for CH₄O (methanol), C₂H₃N
275 (acetonitrile), C₂H₄O (acetaldehyde), C₂H₆O (ethanol), C₆H₆ (benzene), C₇H₈ (toluene), C₃H₃N (acrylonitrile),
276 C₃H₄O (acrolein), C₃H₆O (acetone + propanal), C₈H₁₀ (ethylbenzene + m-, p-, and o-xylenes), and C₄H₆O (methyl
277 vinyl ketone + methacrolein + 2-butenal). However, the NOAA PTR-ToF-MS was higher by a factor of 2 or more
278 for C₂H₆S (dimethyl sulfide), C₄H₅N (pyrrole + butene nitrile isomers), C₄H₄O (furan), C₃H₆O₂ (methyl acetate +
279 ethyl formate + hydroxyacetone), C₅H₆O (2-methyl furan + 3-methyl furan), C₅H₄O₂ (furfural + 3-furaldehyde), and
280 C₁₀H₁₆ (monoterpenes) whereas CH₃NO₂ (nitromethane) agreed with the WAS but was lower than TOGA.

281 The discrepancies between the GC-MS techniques and PTR-ToF-MS for a number of key species, such as furans,
282 generally show that the PTR-ToF-MS measures more signal than what can be accounted for by GC-MS. This
283 observation likely results from a combination of (a) PTR-ToF-MS fragmentation of higher molecular weight gases
284 that produce signals at parent ion masses, (b) the detection of isomers that cannot elute through a GC column, and
285 (c) the detection of molecules that are lost to canister sampling. To investigate the causes of these discrepancies,
286 Table S5 shows isomer distributions for masses detected by the PTR-ToF-MS that are known to represent the sum
287 of two or more overlapping isomers. These isomer distributions are calculated from the ratio of GC-MS
288 measurements to the corresponding PTR-ToF-MS mass. Each ratio represents the fraction of the total signal
289 measured by PTR-ToF-MS that is associated with a given isomer. For example, GC-MS measurements identify 2-
290 methylfuran and 3-methylfuran as the key isomers with the molecular formula C₅H₆O. The slope of isomers to PTR-
291 ToF-MS measurements of C₅H₆O represents the isomer fraction detected by PTR-ToF-MS.

292 The isomer distributions shown in Table S5 are compared to those reported for laboratory smoke by Koss et al.
293 (2018). Koss et al. (2018) assigned PTR-ToF-MS masses based on literature searches, intercomparisons of PTR-
294 ToF-MS measurements to other in situ instrumentation, and offline analysis by coupling GC effluent of sampled
295 smoke to the inlet of the PTR-ToF-MS (combined instrumental setup termed GC-PTR-ToF-MS). For low molecular
296 weight gases known to elute through a GC column, Koss et al. (2018) assigned isomer distributions based on the
297 total signal detected by GC-PTR-ToF-MS, which includes signals from parent ions produced from proton-transfer
298 as well as fragments from higher molecular weight gases that elute through a GC. For example, at C₅H₆O-H⁺ (m/z
299 83.0491), 51% of the signal resulted from the elution of 2-methylfuran, 9% resulted from 3-methylfuran, and 37%
300 was associated with other peaks in the chromatogram that produced signals at C₅H₆O-H⁺ (unidentified isomers +
301 fragments of higher masses). We note that the PTR-ToF-MS instrument employed in this study is the same as that
302 used by Koss et al. (2018) and is operated with the same drift field (E/N = 120 Td).

303 For species measured during FIREX-AQ where the PTR-ToF-MS reported significantly more mass than the GC
304 instruments, we find that the isomer distributions derived in this study significantly differ from those derived by



305 Koss et al (2018) (Table S5). This is most pronounced for the monoterpenes but also the furanoic species, such as
 306 furan (C₄H₄O), methylfurans (C₅H₆O), and furfurals (C₅H₄O₂). Hatch et al. (2017) showed that more than 30
 307 different isomers can contribute to the monoterpenes signal based on two dimensional GC. However, the
 308 conventional GC instruments used during FIREX-AQ could only detect a fraction of these isomers. Furthermore,
 309 differences in sensitivity for the different isomers would further increase the quantification uncertainties for both
 310 GC and PTR-ToF-MS. For the furanoic masses, the PTR-ToF-MS measures a higher fraction of unknown isomers
 311 and fragments than what is reported by Koss et al. (2018). This result holds whether comparing against isomer
 312 distributions derived using TOGA (an online GC method) or WAS methods (a canister sampling method),
 313 suggesting that uncertainties due to differences in calibration or canister effects are small. These results suggest that
 314 the total signal of furans measured by PTR-ToF-MS during FIREX-AQ is likely influenced by gases that cannot
 315 pass through a GC column, which includes the possibility of unidentified isomers and fragments from higher
 316 molecular weight species. We note that this result is not specific to the PTR-ToF-MS used in this study, as the
 317 agreement between the NOAA PTR-ToF-MS and UIBK/UiO PTR-ToF-MS for these masses is within 3% (Table
 318 S5).

319 Furans are an important contributor to VOC reactivity and significantly contribute to the formation of ozone and
 320 other secondary gases (Gilman et al. 2015, Hatch et al. 2017, Coggon et al. 2018). For models employing emission
 321 factors of furans, we recommend using emission factors derived using GC-based methods given that multiple
 322 isomers can be detected with PTR-TOF-MS at the furan mass. This also applies to other specific compound classes.
 323 In Table S1, we include the methods used in this study to derive emission factors. For applications where the fast
 324 time-resolution from PTR-ToF-MS is needed (e.g., in deriving cross-plume trends in gases), (Decker et al. 2021; Xu
 325 et al. 2021), the interpretation of trends in furans should include the possibility of unknown isomers and fragments.

326 3.3 Emission ratios and emission factors of US wildfire smoke

327 The freshest plume transects are used to estimate the primary emissions for individual fires. Table 3 shows the
 328 average compound-specific enhancement ratios to CO which we interpret as emission ratios (ERs) for most species,
 329 and the inferred emission factors (EFs) calculated for more than 100 species and groups of species from the freshest
 330 wildfire plume transects sampled during FIREX-AQ. ERs and EFs for each fire are also calculated and provided in
 331 Tables S2 and S3. Given that fast chemistry already occurred in some fire transects, the ER and EF estimates of
 332 highly reactive species like HONO are lower bounds. ERs are the slope of a linear fit of each species with CO
 333 mixing ratios (see section S1). EFs were calculated following Eq. (1):

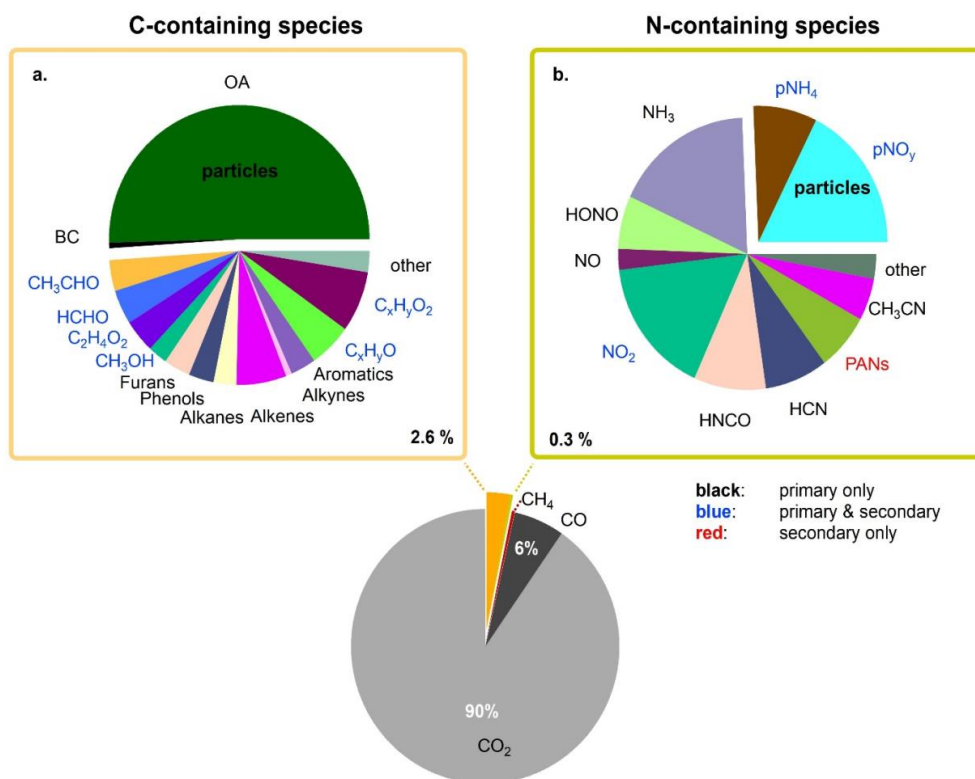
$$334 \quad EF_i = F_C \cdot \frac{MM_i}{AW_C} \cdot \frac{\Delta i/\Delta CO}{\sum_{x=1}^n (NC_x \cdot \frac{\Delta C_x}{\Delta CO})}, \quad (1)$$

335 where EF_{*i*} is the emission factor of compound *i* calculated similarly to Akagi et al. (2011); F_C is the carbon fraction
 336 of the fuel assumed to be 0.5 g g⁻¹; MM_{*i*} is the molar mass of *i*; AW_C is the atomic mass of carbon (12 g mol⁻¹);
 337 Δ*i*/ΔCO is the emission ratio of a compound relative to CO; NC_{*x*} is the number of carbon atoms in C-containing
 338 species *x*, and ΔC_{*x*}/ΔCO is the emission ratio of species *x* to CO. This method assumes that all the carbon lost from
 339 the fuel as it burns is emitted and measured, which is a reasonable approximation as CO, CO₂, and CH₄ account for
 340 most of the emitted carbon (Akagi et al., 2011). The denominator of the last term estimates total carbon relative to
 341 CO. Species C_{*x*} includes all species shown in Table 3. The carbon not quantified by the suite of instrumentation
 342 available during FIREX-AQ likely results in emission factor overestimates no more than 1–2% (Yokelson et al.,
 343 2013; Stockwell et al., 2015).

344 Figure 3 shows the average chemical composition of freshly emitted wildfire smoke in g kg⁻¹ (see Eq. (1)). CO₂,
 345 CO, and CH₄ are 97% of the total mass. The remaining 3% consisted of gas- and particle-phase carbon-containing
 346 (C-containing, 2.6%) and nitrogen-containing (N-containing, 0.3%) species. 50.4% and 0.7% of this remaining C-
 347 containing total mass results from organic aerosol and black carbon (BC), respectively. In the gas phase, 6.4% of
 348 the remaining C-containing species mass, which includes all species in Figure 3a, were phenolic compounds and
 349 furans, 4% formaldehyde (HCHO), 4% glycolaldehyde and acetic acid (C₂H₄O₂), 3.7% acetaldehyde (CH₃CHO),
 350 2.1% methanol, 5.8% remaining compounds with one oxygen atom (C_{*x*}H_{*y*}O), 6.9% remaining compounds with two
 351 oxygen atoms (C_{*x*}H_{*y*}O₂), 3.1% aromatics, 6.3% alkenes, 2.8% alkanes, and 3.3% other species. N-containing species



352 mass, shown in Figure 3b, consisted of organic and inorganic nitrate, and other organic nitro compounds such as
 353 nitroaromatics (pNO_y, 19%) and ammonium (pNH₄⁺, 8.5%) in the particle-phase; whereas, the dominant gas-phase
 354 N-containing species mass was from ammonia (NH₃, 18.5%), followed by nitrogen dioxide (NO₂, 17.5%), isocyanic
 355 acid (HNCO, 8.5%), hydrogen cyanide (HCN, 5%), peroxyacyl nitrates (PANs, 7%), nitrous acid (HONO, 4.8%),
 356 nitric oxide (NO, 2.5%), and others at 3%. The high contribution of NO₂ in comparison to NO and HONO, and the
 357 existence of secondary pollutants, in particular PANs, also indicate that chemistry occurred from the time of
 358 emission to the time of detection. Given the fast conversion of NO and HONO to NO₂ and nitrate, and NH₃ to
 359 particulate ammonium, we also include in Table 3 the conserved quantity of NO_y, as well as NO_x as NO, and NH_x
 360 as NH₃ + particulate ammonium. Emissions of SO_x as SO₂ that include the conversion of SO₂ to particulate sulfate
 361 are discussed in Rickly et al. (2022).



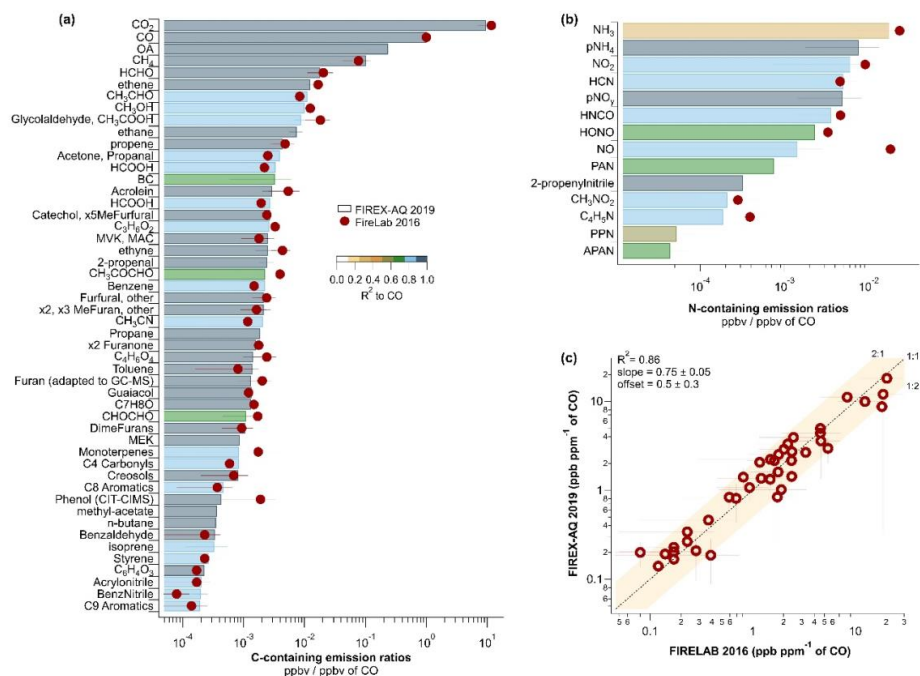
362 **Figure 3:** Pie charts of carbon- and nitrogen-containing species average emission factors (g kg⁻¹) for fresh wildfire smoke. The
 363 text labels indicate compounds with only direct emissions in black, and compounds that are directly emitted and photochemically
 364 produced in blue, and PANs that are only photochemically produced in red, indicating some oxidation even for the freshest
 365 plumes sampled. Although HCHO and CH₃CHO are C_xH_yO species and glycolaldehyde/acetic acid are C_xH_yO₂ species they are
 366 separately presented due to their high abundances.
 367

368 3.4 FIREX-AQ field observations compared to laboratory and field studies

369 The sum of the NMOG EFs sampled during the FIREX-AQ campaign was 23.80 ± 7.5 g kg⁻¹ (3σ), in agreement
 370 with the mean sum from western wildfires during the WE-CAN campaign of 26.1 ± 6.9 g kg⁻¹ (Permar et al., 2021),
 371 temperate forest fires at 23.7 g kg⁻¹ (Akagi et al., 2011) and 24.55 g kg⁻¹ (Andreae, 2019), pine-forest understory
 372 prescribed fires at 27.6 g kg⁻¹ (Yokelson et al., 2013), FLAME-4 laboratory coniferous canopy fires at 23.9 g kg⁻¹
 373 (Stockwell et al., 2015), and FireLab laboratory measurements of various different fuel types at 25 g kg⁻¹ (Koss et



374 al., 2018). The sum of FIREX-AQ NMOG ERs to CO on a molar basis was 135 ± 18 ppb ppm⁻¹, in a similar range
 375 as WE-CAN at 148.3 ± 29.6 ppb ppm⁻¹ and FireLab at 144.5 ppb ppm⁻¹.



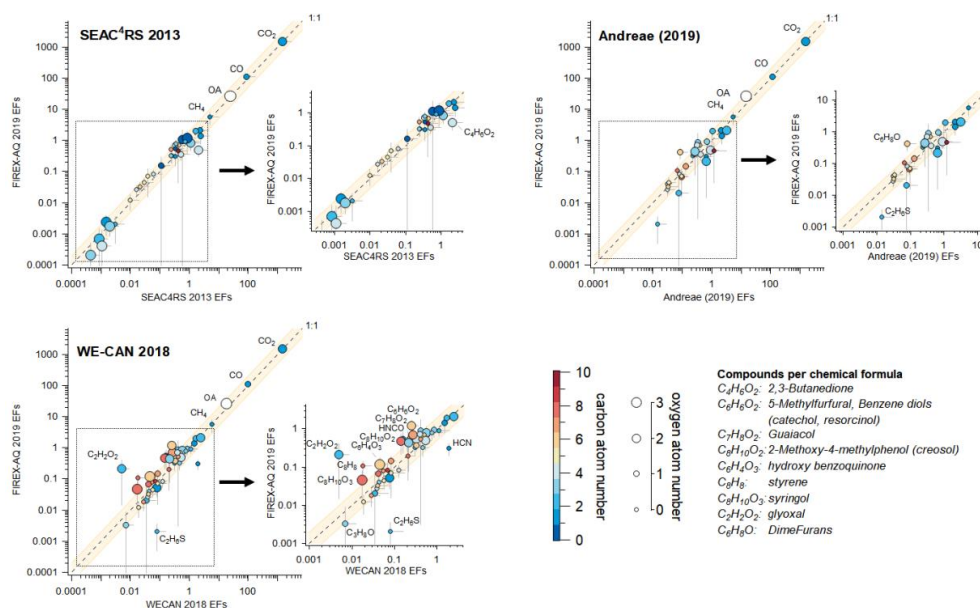
376

377 **Figure 4:** (a) and (b) show the emission ratios for FIREX-AQ (bars) and FireLab (circles) colored by the correlation coefficient,
 378 and (c) direct comparison of FIREX-AQ to FireLab emission ratios for gas-phase species. Error bars in all graphs indicate the 1-
 379 sigma standard deviation. The majority of the observations from FireLab 2016 were calculated using data from the NOAA PTR-
 380 ToF-MS; here we use measurements from the same instrument for FIREX-AQ for more direct comparisons.

381 Figure 4 compares the ERs of C-containing and N-containing compounds (ppb ppm⁻¹ CO) with those measured at
 382 the FireLab (Koss et al., 2018; Selimovic et al., 2018). During FIREX-AQ, all NMOGs correlated well with CO
 383 with correlation coefficients, R^2 , above 0.75, confirming that CO could be used as a proxy for estimating NMOG
 384 emissions close to the fire, as further discussed in Sect. 3.5. Variability in the correlations of individual species with
 385 CO was still evident — for example, species that are both emitted and photochemically produced exhibited lower
 386 correlation (e.g., acetic acid, acetone, and formic acid, $R^2 = 0.75–0.85$) than compounds with only primary emissions
 387 from fires (e.g., aromatics, $R^2 > 0.95$). N-containing species were weakly correlated with CO partly due to varying
 388 fuel N/C (Roberts et al., 2020). In addition, lower correlation of NH_3 could be due to variable amounts of ammonium
 389 formation in aging smoke, or differences in instrument response times between a high volatility compound, such as
 390 CO, compared to NH_3 , which may partition to the inlet and instrument walls before detection (Tomsche et al., 2023;
 391 Stockwell et al., 2014) and slow the instrument response time. Low correlations are also found for HONO, which is
 392 highly reactive and removed by photochemistry (Peng et al., 2020; Theys et al., 2020), as well as for glyoxal and
 393 methylglyoxal, which are photochemically formed and could partition differently to the particle phase depending on
 394 humidity (Mitsuishi et al., 2018; Ling et al., 2020). N-containing species were in good agreement except the higher
 395 contribution of NO and particulate ammonium in Firelab and FIREX-AQ, respectively. This difference reflects the
 396 depletion of NO and the secondary formation of particulate ammonium in field observations and promotes that fast
 397 chemistry of reactive compounds occurred prior to the FIREX-AQ sampling. In summary, variability in post-
 398 emission processes, fuel nitrogen, and fast photochemistry are likely important factors that contribute to the
 399 differences in correlations between FIREX-AQ and Firelab measurements of NMOGs, NO_y species, and CO.



400 While the PTR-ToF-MS is well-suited for detecting NMOGs, it is prone to fragmentation for a range of molecules,
 401 depending on their molecular structure (Pagonis et al., 2019). For such compounds, measurement uncertainties
 402 increase, and comparisons to previous studies that use different instrumentation become more challenging. As
 403 outlined in Sect. 2, the NOAA PTR-ToF-MS used in this study was the same instrument as used in the FireLab three
 404 years prior (Koss et al., 2018). This provided an important opportunity to compare field-derived emissions to
 405 laboratory studies. FireLab average ERs were calculated by comparing similar fuel types as measured during
 406 FIREX-AQ, including Ponderosa Pine, Lodgepole Pine, Douglas Fir, Subalpine Fir, Engelmann Spruce, Loblolly
 407 Pine, Jeffrey Pine, Juniper, Manzanita, Chamise, and Bear Grass laboratory fires. Overall, FIREX-AQ ERs agree
 408 with those from the FireLab within a factor of 2 for most compounds (see Figure S3). Compounds with the largest
 409 differences were benzonitrile with a FIREX-AQ to FireLab ratio of 2.46, ethene (1.88), CH₃CN (1.77), toluene
 410 (1.71), HCOOH (1.64), the sum of acetone and propanal (1.62), glycolaldehyde and acetic acid (0.50), monoterpenes
 411 (0.49), C₄H₅N species (0.47), syringol (0.32), and ethanol (0.28).



412

413 **Figure 5:** Comparison of FIREX-AQ EFs to those from SEAC⁴RS 2013 (Liu et al., 2017), WE-CAN (Permar et al., 2021), and
 414 the review publication by Andreae (2019). Shaded areas show differences within a factor of 2.

415 Figure 5 and Table S6 compare FIREX-AQ observations against field-derived wildfire EFs from SEAC⁴RS (Liu et
 416 al., 2017), WE-CAN (Permar et al., 2021), and literature-average temperate forest EFs from Andreae (2019). For all
 417 studies, the measurements agree within a factor of 2 for 83%, 87%, and 78% of the compounds reported during
 418 SEAC⁴RS, WE-CAN, and the Andreae (2019) temperate forest fires average (includes SEAC⁴RS), respectively.
 419 FIREX-AQ EFs were on average higher compared to previous studies. The average ratio ($\pm 1\sigma$) of FIREX-AQ to
 420 WE-CAN, SEAC⁴RS, and temperate forest fires from Andreae (2019) were 1.42 ± 0.3 , 1.26 ± 0.42 , and 1.24 ± 0.36 ,
 421 respectively (see Table S6). Glyoxal and methylglyoxal were expected to have higher discrepancies due to their
 422 secondary production and RH-dependent particle-phase partitioning, but also due to the higher quantification
 423 uncertainties in the previous studies. For example, during WE-CAN (Permar et al., 2021), a PTR-ToF-MS was used
 424 to detect these compounds, which are prone to fragmentation upon ionization in the PTR-ToF-MS. Furthermore,
 425 the calculated glyoxal sensitivity used by Permar et al. (2021) was high (Stöner et al., 2016) and could therefore lead
 426 to a significant underestimation. In this study, glyoxal and methylglyoxal were measured by cavity-enhanced
 427 spectroscopy, and the uncertainties were $< 5\%$ (see Sect. 2). Furthermore, comparison of the FIREX-AQ to the
 428 FireLab EFs also measured by the same spectroscopic technique (see Figure 4) (Zarzana et al., 2018) showed that
 429 glyoxal and methylglyoxal were in better agreement with FIREX-AQ compared to Permar et al. (2021) but still



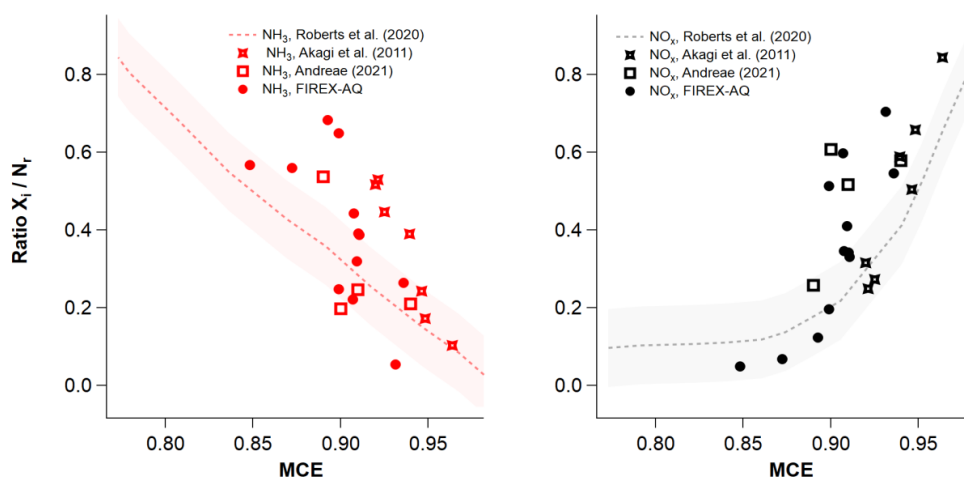
430 lower by 50% and 75%, respectively. Dimethyl sulfide (DMS) is a compound that originates predominantly from
431 oceanic emissions and its fire emissions were lower for this study compared to WE-CAN and the temperate forest
432 fire emissions average, but higher by 20% compared to the SEAC⁴RS EFs. FIREX-AQ monoterpenes were higher
433 than those in WE-CAN and Firelab by a factor of 2, and lower than the temperate forest fire emissions average
434 (Andreae 2019) by a factor of 2, which likely stems from the large variability of monoterpene emissions for different
435 fuel types and the difficulties inherent with the large number of isomers (Hatch et al. 2017; Koss et al. 2018;
436 Sekimoto et al. 2018). OA was 50% higher compared to WE-CAN and temperate forest fire emissions, but within
437 10% when compared to the SEAC⁴RS OA emissions. The variability of OA EFs highlights the importance of
438 accounting for the partitioning and aging of OA when comparing OA EFs across biomass burning campaigns given
439 that fraction of the detected OA from wildfire plumes can be a mix of primary and secondary (Pagonis et al., 2020).

440 Focusing on the two large recent campaigns dedicated to wildfires we note that differences can occur due to natural
441 variability with 2018 being a more intense fire season (Jin et al., 2023), but also from the different fragmentation,
442 inlet setups, and quantification uncertainties between the instruments used. Differences between the WE-CAN and
443 FIREX-AQ EFs for oxygenated compounds could be due to the different quantification uncertainties between the
444 two PTR-ToF-MS instruments. For both studies and instruments, assuming similar isomer sensitivities and no
445 fragmentation interferences, sensitivities for calibrated compounds introduced a 15% uncertainty, whereas
446 sensitivities for uncalibrated species were estimated following theoretical methods described by Sekimoto et al.
447 (2017), which have an uncertainty of 50%. Several reactive oxygenated compounds that have implications for NO_x
448 loss processes such as the formation of nitrophenolic compounds (Finewax et al., 2018; Decker et al., 2021) were
449 calibrated during FIREX-AQ but only calculated during WE-CAN, such as C₇H₈O (o-cresol, anisol), C₇H₈O₂
450 (guaiacol), and C₈H₁₀O₂ (creosol). One mass calibrated on both instruments was C₆H₆O₂ (sum of 5-methyl furfural,
451 catechol, resorcinol), but was still a factor of 5 higher during FIREX-AQ compared to WE-CAN. However, the
452 FIREX-AQ ERs for C₆H₆O₂ agreed within 45% of the FireLab study, which used the same instrument, suggesting
453 possible differences in fragmentation or isomer assignment between the FIREX-AQ and WE-CAN instruments.
454 Styrene (C₈H₈) from FIREX-AQ (using PTR-MS) was a factor of 6 higher compared to the WE-CAN measurements
455 (GC-MS) but agreed within 60% with SEAC⁴RS (GC-MS) and FireLab EFs (PTR-MS). C₆H₈O (sum of 2,5-
456 dimethylfuran, 2-ethylfuran, and other C₂-substituted furan isomers), C₈H₁₀O₃ (syringol), and C₆H₄O₃ (hydroxy
457 benzoquinone) were quantified using estimated calibration factors during both campaigns, and therefore more
458 uncertain, and were higher by a factor of 2–5 during FIREX-AQ. Another influencing factor for the overall higher
459 EFs for oxygenated compounds during FIREX-AQ could be due to the optimized inlet setups to limit wall losses
460 prior to detection for the majority of the instruments (Table 2). Various oxygenated compounds are more sticky and
461 can therefore partition to the inlet line walls prior to their detection. For example, during FIREX-AQ the NOAA
462 PTR-ToF-MS inlet line was 1-m long and heated at 60°C to reduce condensation sinks resulting in less than 1 s
463 residence times; in Firelab (Koss et al., 2018) a longer 16 m transfer line was used at 40°C with a residence time
464 comparable to FIREX-AQ whereas in WE-CAN (Permar et al., 2021) the smoke to drift tube time was higher (~ 2
465 s) at temperatures of 55-60°C. This could therefore contribute to differences for larger or more oxygenated NMOGs
466 between campaigns and partly explain the overall increased EFs during FIREX-AQ.

467 Further differences between FIREX-AQ and WE-CAN may also result from the methods used to identify and
468 characterize young plumes. As described in Section 3.1, fresh plumes are identified during FIREX-AQ based on
469 chemical aging proxies, whereas fresh plumes identified in WE-CAN are based on physical distance downwind. For
470 highly reactive species, such as furans and oxygenated aromatics, strong fire-to-fire variability in OH exposure may
471 alter emission factors, even in smoke with similar downwind age. Figure S2 compares the FIREX-AQ and WE-
472 CAN field observations to the ERs obtained during the FireLab laboratory study for a variety of overlapping NMOGs
473 with varying reactivities towards OH radicals. Given that FireLab experiments were performed under dark and
474 warmer conditions in smoke aged just 5 s, it is expected that the more reactive compounds would show higher ERs
475 when compared to field observations if the sampled smoke onboard the aircraft was already aged. However, higher
476 ERs were observed for various compounds measured during FIREX-AQ. On the contrary, when comparing WE-
477 CAN to FireLab ERs, the highly reactive compounds were lower although the ERs of less reactive compounds were
478 in good agreement. This indicates possible differences between FIREX-AQ and WE-CAN owing to variability in
479 chemical oxidation, which has the largest impact on highly reactive species.



480 The correlation to MCE for each species EFs was calculated for all wildfires as shown in Table S4 and compared to
 481 the WE-CAN observations. Correlation coefficients (R^2) during FIREX-AQ were above 0.5 for 28% of the species,
 482 0.3–0.5 for 27% of the species, and below 0.3 for the remaining species. The lowest correlations, below 0.1, were
 483 found for N-containing species, including particulate ammonium and pNOy, ammonia, acetonitrile, 2-butyl nitrate,
 484 methyl nitrate, pyrrole and butene nitrile isomers, and acrylonitrile. Nevertheless, agreement within a factor of 2
 485 was found when compared to the slopes and R^2 obtained from the WE-CAN campaign for most of the compounds.
 486 Figure 6 shows the dependence of two N-containing species on fire MCEs for the FIREX-AQ and FireLab (Roberts
 487 et al., 2020) studies as well as for a majority of fuel types by Akagi et al. (2011) and Andreae (2019). We report N-
 488 containing species as a ratio to the total reactive nitrogen N_r , defined as the sum of NO, NO₂, HONO, HNCO, HCN,
 489 NH₃, other N-containing VOCs, and particle-phase nitrate and ammonium. The dotted lines and shaded regions
 490 show FireLab parameterizations that describe how these ratios respond to changes in MCE (Roberts et al., 2020) for
 491 one fire burned during FireLab whereas square and bended square markers indicate different land cover types from
 492 Andreae (2019) and Akagi et al. (2011), respectively. It should be noted that for Akagi et al. (2011) and Andreae
 493 (2019) N_r measurements are limited to the sum of NO, NO₂, HONO, HCN, and NH₃ and therefore the N_r could
 494 represent a lower limit. For both laboratory and field studies and independent of the fuel burnt, as MCE increases,
 495 NO_x/ N_r increases, whereas NH₃/ N_r decreases. The FireLab MCE ranged from pure flaming (MCE = 0.99) to
 496 smoldering values (MCE < 0.8), but ambient observations during FIREX-AQ were limited to MCE values ranging
 497 from 0.85 to 0.95, which suggests both flaming and smoldering contributions to the sampled wildfire plumes.



498

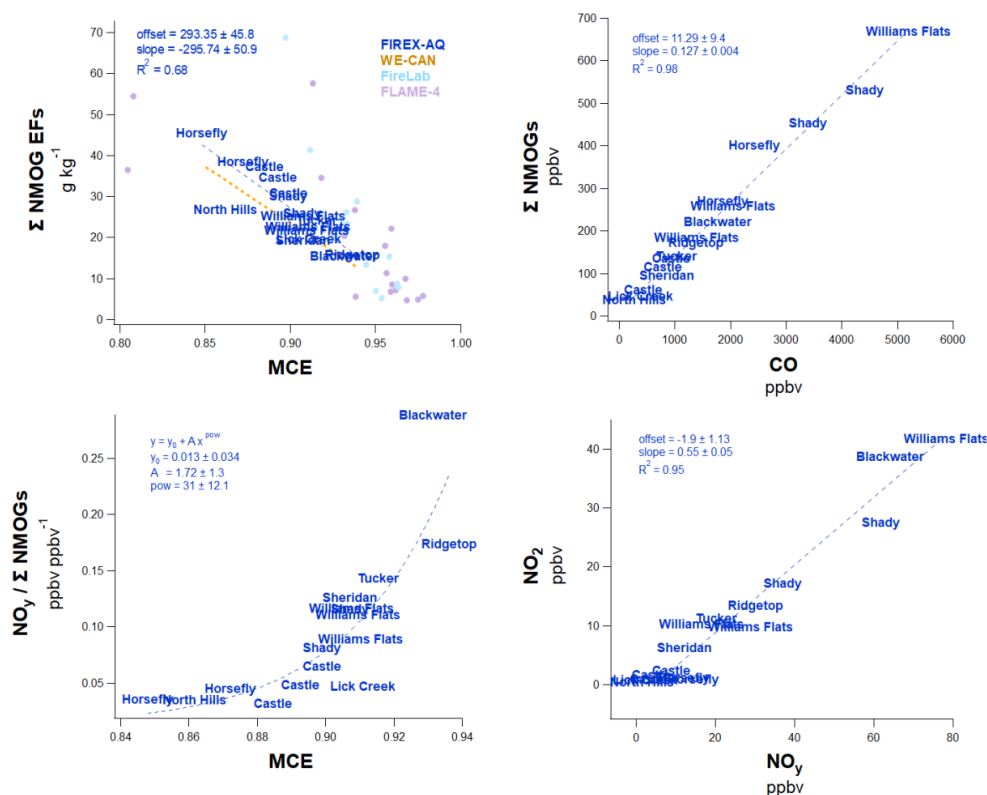
499 **Figure 6:** Ratios of two N-species to the total nitrogen, N_r , during FIREX-AQ compared to Roberts et al. (2020) based on one
 500 fire burned during FireLab, and Andreae (2019) and Akagi et al. (2011) that include different land cover types.

501 3.5 Parameterization of organic- and nitrogen-containing emissions in wildfire plumes

502 The comparisons described above demonstrate that FIREX-AQ emissions agreed within a factor of 2 or better with
 503 previous laboratory and field studies for most C- and N-containing species for temperate ecosystem fuels. In the
 504 following, we relate primary wildfire emissions and emission factors to fire emissions measurable from space, e.g.,
 505 CO (e.g., Schneising et al., 2020), NO₂ (e.g., Martínez-Alonso et al., 2020), and BC (e.g., Kononov et al., 2018),
 506 as well as MCE. Although current satellite retrievals for wildfire smoke can agree with airborne observations e.g.,
 507 for NO_x and CO (Griffin et al., 2021; Stockwell et al. 2022), challenges in isolating the fire contribution from small
 508 or short-lived fires, as well as cloud coverage and aerosol interferences, add uncertainties to this quantification (e.g.,
 509 Jung et al., 2019; Vasilkov et al., 2021). Here, we only focus on the parameterization of wildfire plumes and promote
 510 future efforts to quantify these compounds using satellite retrievals more accurately. Satellite-retrieved
 511 concentrations of CO and NO₂ close to wildfires could then be used to estimate NMOG and NO_y emissions and
 512 potentially better account for variability associated with fire emissions and improve modeling efforts to simplify
 513 and predict downwind formation of secondary pollutants, including ozone and secondary organic aerosol.



514 Figure 7 shows correlations between the sum of the median mixing ratios of NMOGs and NO_y with MCE, CO, and
 515 NO_2 , where CO and NO_2 are two species available from satellite products that could be used as proxies for
 516 smoldering and flaming combustion (e.g., van der Velde et al., 2021; Urbanski et al., 2008), respectively. Figure 7a
 517 shows that the sum of FIREX-AQ NMOG EFs correlated with MCE with an R^2 of 0.68, even though many of the
 518 individual compounds are poorly correlated with MCE (Table S4). The correlation of the FIREX-AQ MCE to the
 519 sum of NMOGs was in the same range as WE-CAN, FireLab, and FLAME-4 observations. WE-CAN was
 520 consistently lower, by around 10%, which is partially due to differences in the assumed fraction of carbon employed
 521 in Eq. (1) (45.7% for WE-CAN and 50% for this study). FIREX-AQ sampled fires with lower MCEs on average
 522 than the lab experiments, with lab experiments showing highly variable EFs for MCE values below 0.9. Additional
 523 reasons for different FireLab and FLAME-4 EFs vs. MCE are discussed in detail by Permar et al. (2021) and include,
 524 (1) rapid chemistry prior to sampling, which results in the degradation of short-lived species (Figure S2) and/or less
 525 partitioning to particles at higher lab temperatures, (2) laboratory studies may more efficiently sample smoldering
 526 combustion emissions compared to aircraft observations where residual smoldering combustion emissions might
 527 not be lofted and therefore undersampled at the aircraft altitude, and (3) laboratory MCEs are often higher than in
 528 the field due to experimental conditions, including drier fuel and more efficient burning conditions (Yokelson et al.,
 529 2013; Holder et al., 2017; Selimovic et al., 2018), whereas field MCEs are calculated from single transects through
 530 smoke plumes that likely contain a different mix of flaming vs. smoldering (Wiggins et al., 2020). Nevertheless, the
 531 good agreement between two different aircraft studies during different years and the general agreement with FireLab
 532 and FLAME-4 study averages further highlight the consistency of total NMOG correlations with MCE in wildfire
 533 emissions despite the poorer correlations of individual compounds with MCE (Table S4).



534

535 **Figure 7:** Correlation trends observed for western US wildfire emissions for (a) the sum of median NMOG EFs compared to
 536 MCE for each wildfire. Each data point represents one fire from either FIREX-AQ, WE-CAN (Permar et al., 2021), FireLab
 537 (Koss et al., 2018), or FLAME-4 (Stockwell et al., 2015) with the name of each FIREX-AQ fire centered on the data points. (b)



538 Sum of median NMOG mixing ratios plotted vs. CO, (c) ratio of median NO_y species to the sum of NMOGs vs. MCE, and (d)
 539 median NO_y mixing ratios vs. the median NO₂ concentration. Dashed lines indicate linear fits for (a), (b), and (d), and a power
 540 function fit for (c).

541 Figure 7b relates the sum of the median NMOG mixing ratios to the median CO mixing ratios for all the freshest
 542 sampled wildfire plumes. CO results largely from smoldering combustion, which is the combustion process that also
 543 produces most NMOGs. NMOGs and CO are very well correlated, with a slope of 127 ± 4 (ppb ppm⁻¹) and an R²
 544 of 0.98, which demonstrates that total primary NMOG emissions are effectively represented by CO. Figure S4 shows
 545 that R² values with CO for individual compounds were above 0.9 for the majority of primary NMOGs reported here,
 546 whereas, for secondary species, the correlations were below 0.3. CO columns are retrievable from space by, e.g.,
 547 TROPOMI (Martínez-Alonso et al., 2020) and CRiS (NASA, 2015) and can be used to derive CO emissions that
 548 generally agree with *in situ* observations (Stockwell et al. 2022). The correlations from the FIREX-AQ
 549 measurements and others could be used to initialize total NMOG emissions from wildfire plumes in models.

550 Quantification of N-containing species is also essential for understanding and modeling the evolution and formation
 551 of secondary organic aerosol and ozone downwind of wildfires. Figure 7c shows the ratio of measured NO_y by the
 552 chemiluminescence instrument (see Section 2.1), to the sum of NMOGs in ppb ppb⁻¹. A rapid increase in this ratio
 553 is observed as MCE increases described by a power function fit. This increase follows the expectation that as fires
 554 transition from smoldering to flaming conditions, MCE increases, NMOGs EFs decrease, and fuel nitrogen leads to
 555 the formation of NO_x through radical chemistry of N-containing compounds (Roberts et al., 2020). Figure 7d shows
 556 that NO₂ represents a significant fraction of NO_y with a slope of 0.55 ± 0.03 (ppb ppb⁻¹) and an R² of 0.95.
 557 Furthermore, the correlation of individual N-containing species with NO₂ is significantly higher than their
 558 correlation with CO mixing ratios (Figure S4) promoting that NO₂ measurements could be used to initialize total
 559 NO_y emissions and N-species from wildfire plumes in models. Figures S5 shows additional correlations that could
 560 be used for modeling efforts, including the correlation of NO_y to CO, NO_y to BC, and others.

561 These observations suggest that CO is a good proxy for species emitted from western wildfires primarily during
 562 smoldering conditions (i.e., NMOGs), whereas NO₂ is a good proxy for species that are mostly emitted during
 563 flaming conditions (i.e., mostly NO_y). Thus, in addition to coupling EFs with fuel consumption to derive emissions,
 564 we suggest future use of satellite retrievals close to the fire plume to quantify CO and NO₂ concentrations in order
 565 to accurately determine EFs for all carbon and nitrogen-containing species for western US wildfire plumes as input
 566 to models. An important assumption, especially in determining emissions of N-containing species, is that NO₂
 567 should accurately represent NO_y close to the fire. However, satellite retrievals that capture truly fresh emissions very
 568 close to the fire will be dominated by NO and HONO whereas in highly oxidized plumes NO₂ loss processes will
 569 lower its overall contribution to NO_y. It is therefore important to provide a range of distances where this holds true.
 570 Coggon et al. (2022) find that for fires with highly reactive emissions, NO₂ represents NO_y within the first 15-30
 571 min and a distance of 10-20 km downwind of the fire assuming a wind speed 10 m/s. Current satellite retrievals for
 572 wildfire smoke have a spatial resolution of 3.5 km×5.5 km (Griffin et al., 2021) which would be within the above
 573 range and high enough to represent plumes where NO₂ is the dominant fraction of NO_y.

574 **Table 3:** Emission ratios and emission factors of organic and nitrogen compounds from wildfire plumes. In blue are multiple
 575 isomers measured as sum by the NOAA PTR-ToF-MS that were further speciated based on other GC-MS measurements from
 576 FIREX-AQ (column 1 in parenthesis). Here, we show the ratio of each isomer measured by GC-MS to the total PTR-ToF-MS
 577 signal obtained in this mass.

Compound <i>Isomer contribution to each mass is provided in parenthesis based on the ratio of each isomer measured by GC-MS to the sum measured by PTR-ToF-MS (check Table S5)</i>	Instrument	Exact Mass, Da	Chemical formula/structure	EFs (g kg ⁻¹)	± σ	ERs (ppb ppm ⁻¹)	± σ
Gas-Phase							
Carbon dioxide	DACOM	43.99	CO ₂	1533.82	78.06	9400.32	2455.30



Carbon monoxide	DACOM	27.99	CO	109.15	22.70	1000.00	0.00
Methane	DACOM	16.03	CH ₄	5.81	2.68	91.97	31.61
Formaldehyde	CAMS & ISAF	30.01	CH ₂ O	2.10	0.79	17.92	4.31
Acetic acid + Glycolaldehyde	NOAA PTR-ToF-MS for the sum	60.02	C ₂ H ₄ O ₂	2.09	0.61	8.86	1.51
Acetaldehyde	NOAA PTR-ToF-MS	44.03	C ₂ H ₄ O	1.95	0.60	11.25	1.70
Ethene	iWAS	28.03	C ₂ H ₄	1.52	0.45	13.57	1.97
Methanol	NOAA PTR-ToF-MS	32.03	CH ₄ O	1.42	0.66	10.90	3.21
5-Methylfurfural + Benzene diols (=Catechol, Resorcinol)	NOAA PTR-ToF-MS for the sum	110.11	C ₆ H ₆ O ₂	1.20	0.47	2.72	0.68
Acetone (78%) + Propanal (22%)	NOAA PTR-ToF-MS (speciation by GC-MS)	58.04	C ₃ H ₆ O	0.93	0.34	4.04	0.84
Ethane	iWAS	30.05	C ₂ H ₆	0.91	0.26	7.76	1.84
Methyl acetate + Ethyl formate + Hydroxyacetone	NOAA PTR-ToF-MS for the sum	74.04	C ₃ H ₆ O ₂	0.81	0.36	2.70	0.73
Propene	iWAS	42.05	C ₃ H ₆	0.80	0.27	4.80	1.16
MVK (38%) + Methacrolein (27%) + 2-Butenal (33%)	NOAA PTR-ToF-MS (speciation by GC-MS)	70.09	C ₄ H ₆ O	0.71	0.27	2.56	0.56
Benzene	NOAA PTR-ToF-MS	78.05	C ₆ H ₆	0.69	0.17	2.26	0.24
Guaiacol (=2-Methoxyphenol)	NOAA PTR-ToF-MS	124.14	C ₇ H ₈ O ₂	0.70	0.34	1.38	0.52
Acrolein	NOAA PTR-ToF-MS	56.03	C ₃ H ₄ O	0.88	0.88	3.73	2.73
Methyl glyoxal	ACES	72.06	CH ₃ COCHO	0.44	0.36	1.55	1.23
Isocyanic acid	NOAA PTR-ToF-MS	43.01	HNCO	0.53	0.31	3.51	2.46
Formic acid	NOAA PTR-ToF-MS	46.00	HCOOH	0.60	0.43	3.31	1.95
2-Methylphenol (=o-cresol) + Anisol	NOAA PTR-ToF-MS for the sum	108.14	C ₇ H ₈ O	0.57	0.22	1.32	0.37
2-(3H)-Furanone	NOAA PTR-ToF-MS	84.02	C ₄ H ₄ O ₂	0.54	0.26	1.60	0.50
HCN	CIT-CIMS	27.01	HCN	0.31	0.12	3.01	1.08
Toluene	NOAA PTR-ToF-MS	92.06	C ₇ H ₈	0.53	0.21	1.42	0.35
2,3-Butanedione + 2-Oxobutanal + 1,4-Butanedial	NOAA PTR-ToF-MS for the sum	86.04	C ₄ H ₆ O ₂	0.49	0.20	1.43	0.37
Monoterpenes	NOAA PTR-ToF-MS	136.24	C ₁₀ H ₁₆	0.47	0.43	0.82	0.65
2-Methoxy-4-methylphenol (= Creosol)	NOAA PTR-ToF-MS	138.16	C ₈ H ₁₀ O ₂	0.47	0.26	0.82	0.36
2,5-Dimethylfuran + 2-Ethylfuran + Other unidentified organic compounds	NOAA PTR-ToF-MS for the sum	96.06	C ₆ H ₈ O	0.41	0.16	1.07	0.27
Phenol	CIT-CIMS	94.04	C ₆ H ₆ O	0.16	0.05	0.43	0.13
Furan	TOGA	68.03	C ₄ H ₄ O	0.35	0.13	1.33	0.40
i-Butene	iWAS	56.06	C ₄ H ₈	0.35	0.12	1.61	0.42
Acetonitrile	NOAA PTR-ToF-MS	41.03	C ₂ H ₃ N	0.32	0.14	2.04	0.86
Propane	iWAS	44.06	C ₃ H ₈	0.33	0.14	1.90	0.66
Ethyne	iWAS	26.02	C ₂ H ₂	0.30	0.14	2.90	0.92
Glyoxal	ACES	58.04	CHOCHO	0.22	0.20	0.94	0.78
MEK	NOAA PTR-ToF-MS	72.06	C ₄ H ₈ O	0.24	0.08	0.84	0.20
Ethylbenzene (7%) + m- and p-Xylenes (58%) + o-Xylene (21%)	NOAA PTR-ToF-MS (speciation by GC-MS)	106.17	C ₈ H ₁₀	0.08	0.04	0.18	0.07



2-Furfural	TOGA	96.02	C5H4O2	0.18	0.06	0.47	0.11
Benzaldehyde	NOAA PTR-ToF-MS	106.12	C7H6O	0.15	0.05	0.35	0.06
Butene	iWAS	56.06	C4H8	0.15	0.05	0.68	0.16
Hydroxy benzoquinone	NOAA PTR-ToF-MS	124.09	C6H4O3	0.12	0.06	0.23	0.09
2-Methylfuran	TOGA	82.04	C5H6O	0.11	0.04	0.34	0.10
Styrene	NOAA PTR-ToF-MS	104.15	C8H8	0.11	0.04	0.26	0.06
C9 Aromatics	NOAA PTR-ToF-MS	120.19	C9H12	0.084	0.043	0.178	0.073
Naphthalene	NOAA PTR-ToF-MS	128.17	C10H8	0.077	0.032	0.161	0.074
n-Butane	iWAS	58.08	C4H10	0.082	0.030	0.368	0.121
Benzonitrile	NOAA PTR-ToF-MS	103.04	C7H5N	0.081	0.027	0.200	0.062
Pentene	iWAS	70.08	C5H10	0.073	0.023	0.268	0.069
Benzofuran	NOAA PTR-ToF-MS	118.10	C8H6O	0.067	0.023	0.143	0.031
Butanal	TOGA	72.06	C4H8O	0.060	0.019	0.217	0.064
Isoprene	iWAS	68.06	C5H8	0.070	0.055	0.271	0.203
Propyne	WAS	40.03	C3H4	0.057	0.027	0.362	0.121
2-Methyl-1-butene	iWAS	70.08	C5H10	0.055	0.020	0.201	0.054
Nitromethane	NOAA PTR-ToF-MS	61.02	CH3NO2	0.052	0.025	0.228	0.116
1-Hexene	WAS	84.09	C6H12	0.049	0.013	0.151	0.043
2-Methylpropanal	TOGA	72.06	C4H8O	0.046	0.015	0.167	0.049
n-Pentane	iWAS	72.09	C5H12	0.044	0.018	0.159	0.058
Acrylonitrile	NOAA PTR-ToF-MS	53.03	C3H3N	0.040	0.011	0.202	0.073
Cis-2-Butene	iWAS	56.06	C4H8	0.013	0.005	0.045	0.013
2-Methyl-1-Butene	iWAS	70.08	C5H10	0.055	0.020	0.201	0.054
Syringol	NOAA PTR-ToF-MS	154.17	C8H10O3	0.047	0.034	0.078	0.056
Pentadiene	iWAS	68.06	C5H8	0.033	0.015	0.123	0.044
Trans-2-Butene	iWAS	56.06	C4H8	0.037	0.020	0.166	0.082
n-Hexane	iWAS	86.11	C6H14	0.033	0.013	0.099	0.038
i-Butane	iWAS	58.08	C4H10	0.027	0.010	0.122	0.038
1-Heptene	WAS	98.11	C7H14	0.026	0.008	0.069	0.022
Ethanol	NOAA PTR-ToF-MS	46.04	C2H6O	0.020	0.055	0.098	0.273
n-Nonane	iWAS	128.16	C9H20	0.025	0.010	0.051	0.020
Methyl Formate	iWAS	60.02	C2H4O2	0.020	0.022	0.089	0.095
n-Decane	iWAS	142.17	C10H22	0.023	0.012	0.042	0.024
3-Methylfuran	TOGA	82.04	C5H6O	0.019	0.006	0.058	0.017
1-Octene	WAS	112.13	C8H16	0.018	0.005	0.042	0.013
3-Furfural	TOGA	96.02	C5H4O2	0.018	0.006	0.047	0.011
Trans-2-Pentene	iWAS	70.08	C5H10	0.018	0.008	0.065	0.025
2,4-Dimethylpentane	iWAS	100.13	C7H16	0.018	0.009	0.046	0.019
1-Nonene	WAS	126.14	C9H18	0.015	0.005	0.031	0.011
1-Buten-3-yne	WAS	52.03	C4H4	0.014	0.007	0.070	0.026
Pyrrrole	TOGA	67.04	C4H5N	0.012	0.005	0.047	0.024
i-Pentane	iWAS	72.09	C5H12	0.012	0.006	0.045	0.023
cis-2-Butene	iWAS	70.08	C5H10	0.013	0.005	0.045	0.013
Butene nitrile isomers	TOGA	67.04	C4H5N	0.007	0.003	0.028	0.014
2-Methylpentane	iWAS	86.11	C6H14	0.007	0.003	0.020	0.008
1-Butyne	WAS	54.05	C4H6	0.006	0.003	0.030	0.012



Methylcyclopentane	iWAS	84.09	C6H12	0.005	0.002	0.015	0.006
Methylcyclohexane	iWAS	98.11	C7H14	0.004	0.002	0.011	0.006
Dimethyl sulfide (50%) + other unidentified organic compounds (50%)	NOAA PTR-ToF-MS (speciation by GC-MS)	62.02	C2H6S	0.002	0.002	0.009	0.007
2-Butyne	WAS	54.05	C4H6	0.003	0.002	0.014	0.008
Methyl Nitrate	iWAS	77.01	CH3NO3	0.002	0.002	0.008	0.005
i-Propanol	iWAS	60.06	C3H8O	0.003	0.006	0.015	0.026
i-Propyl nitrate	iWAS	105.04	C3H7NO3	0.002	0.001	0.005	0.002
1,3-Butadiyne	WAS	50.02	C4H2	0.001	0.001	0.006	0.002
Ethyl nitrate	iWAS	91.03	C2H5NO3	0.001	0.001	0.002	0.002
2-Butyl nitrate	iWAS	119.06	C4H9NO3	0.0005	0.001	0.001	0.002
NOy	CL		NOy			12.10	7.38
Nitrogen dioxide	CL	46.01	NO2	1.09	1.22	6.05	5.34
Nitric oxide	CL	30.01	NO	0.16	0.16	1.42	1.44
Nitrous acid	NOAA CIMS	47.00	HONO	0.30	0.21	1.89	1.61
Ammonia	Oslo PTR-ToF-MS	17.03	NH3	1.15	0.77	17.44	11.65

Aerosol-Phase (all units in g/kg)

Organic aerosol (OA/OC = 1.85 ± 0.16)	AMS		OA	26.51	13.97	317.3	148.9
Particulate nitrate	AMS	62.00	pNO _y	1.19	0.78	7.29	2.69
Particulate ammonium	AMS	18.04	pNH ₄ ⁺	0.53	0.37	3.24	1.97
Black carbon	SP2		BC	0.35	0.32	3.26	2.69

Sums

NH _x as NH ₃ (EF _{NH₃} + (17/18) * EF _{NH₄})	UIBK/UiO PTR-ToF-MS + AMS	17.03	NH ₃	1.65	1.14	24.56	17.10
NO _x as NO (EF _{NO} + (30/46) * EF _{NO₂})	CL	30.01	NO	0.87	0.96	5.37	4.92
SO _x as SO ₂	NO-LIF, AMS		See Rickly et al. (2022)				
Total NMOGs emissions				23.80	7.5	135.02	18.23

578

579

Conclusions

580 We present ERs and EFs for NMOGs and nitrogen-containing compounds from nine western US wildfires and one
 581 southeastern US prescribed fire derived from data obtained aboard the NASA DC-8 during the 2019 FIREX-AQ
 582 mission. ERs and EFs were calculated for a total of 16 crosswind plume transects chosen to represent the freshest
 583 fire emissions. These transects were identified based on proxies (e.g., maleic anhydride/furan ratio) for chemical
 584 aging, which can be rapid in fire plumes.

585 We performed detailed comparisons of FIREX-AQ emissions to previous laboratory and field studies with a focus
 586 on oxygenated organic compounds that were calibrated during this mission. FIREX-AQ ERs agree within a factor
 587 of 2 to the FireLab study for most compounds, with a correlation slope of 0.75 ± 0.05 and an R^2 of 0.86. A
 588 comparison of the field-derived EFs from FIREX-AQ with those from SEAC⁴RS (Liu et al., 2017), WE-CAN
 589 (Permar et al., 2021), and temperate forest ERs from Andreae (2019) also agreed to within a factor of 2 for 87%,
 590 83%, and 78% of the compounds, respectively. However, FIREX-AQ EFs are on average higher compared to



591 previous studies. For compounds that agree within a factor of 2, the average ratios of FIREX-AQ to WE-CAN,
592 SEAC4RS, and the temperate forest fire literature average are 1.09 ± 0.3 , 1.25 ± 0.33 , and 1.18 ± 0.4 , respectively,
593 whereas for the remaining compounds, the ratios increase to 2.1 ± 1.64 , 1.29 ± 1.01 , and 1.32 ± 1.23 . We suggest
594 that these differences could be due to differences in the fuel, quantification methods applied for each study, as well
595 as due to differences in photochemical loss of reactive species prior to detection. We further compare the ratio of
596 N-containing species to the total nitrogen (N_i/N_T) vs. MCE and find that NO_x/N_T and NH_3/N_T follow similar trends
597 as those reported by Roberts et al. (2020).

598 We relate wildfire emissions of C- and N-containing species to CO, NO_2 , BC, and MCE based on correlations for
599 use in chemical transport models. Results show that the sum of NMOG EFs correlates with MCE, with an R^2 of 0.68
600 and a slope of -296 ± 51 g kg^{-1} . A better correlation is observed between the sum of the median NMOG mixing
601 ratios and median CO, with a slope of 0.127 ± 0.004 (ppb ppm $^{-1}$) and an R^2 of 0.98. Consistent correlation of
602 individual NMOGs to CO is also evident for the majority of NMOGs with R^2 values greater than 0.9, suggesting
603 significant potential for estimating wildfire NMOG emissions using space-based CO emissions.

604 For N-containing species, the sum of reactive nitrogen, NO_y , correlates better with NO_2 ($R^2 = 0.95$, slope = $1.74 \pm$
605 0.1 ppbv ppbv $^{-1}$) and BC ($R^2 = 0.88$) than with CO ($R^2 = 0.7$) close to the wildfire. Furthermore, the ratio of NO_y
606 to the sum of NMOGs increases exponentially as MCE increases. This further highlights the important influence of
607 fire behavior e.g., flaming vs. smoldering fire conditions on the emissions of reactive nitrogen species. Future efforts
608 to initialize models using the above emissions parameterization could improve the representation of fire emissions
609 in models and their predictions on the downwind formation of secondary pollutants like ozone and secondary organic
610 aerosol.

611 Acknowledgments

612 We would like to thank the NOAA/NASA FIREX-AQ science and aircraft operation teams. GIG, MMC, CES, MMB, IB,
613 JMK, AL, SAM, JAN, JP, PSR, MAR, RHS, CCW, and CW were supported by the NOAA Cooperative Agreement with
614 CIRES, NA17OAR4320101. RY and VS acknowledge NOAA grant NA16OAR4310100 and NSF grant 1748266. JL,
615 GMW, RAH, JMS, and TFH acknowledge support from the NASA Tropospheric Composition Program and NOAA
616 Climate Program Office's Atmospheric Chemistry, Carbon Cycle and Climate (AC4) program (NA17OAR4310004). DP,
617 BAN, HG, PCJ, DAD, MKS, and JLJ were supported by NASA grants 80NSSC18K0630 and 80NSSC21K1451. AF was
618 supported by NASA TCP Grant No. 80NSSC18K0628. The University of Innsbruck team was supported by the Austrian
619 Federal Ministry for Transport, Innovation, and Technology (bmvit, FFG, ASAP). FP received funding from the European
620 Union's Horizon 2020 research and innovation program under grant agreement No. 674911 (IMPACT EU ITN). LX, KTV,
621 HA, JDC, and POW acknowledge NASA grant 80NSSC18K0660 and 80NSSC21K1704. This material is based upon work
622 supported by the National Center for Atmospheric Research, sponsored by the National Science Foundation under
623 Cooperative Agreement No. 1852977.

624
625 **Competing Interests:** AEP and SSB are contributing editors to Atmospheric Chemistry and Physics.

627 References

- 628 Akagi, S. K., Yokelson, R. J., Wiedinmyer, C., Alvarado, M. J., Reid, J. S., Karl, T., Crouse, J. D., and Wennberg, P.
629 O.: Emission factors for open and domestic biomass burning for use in atmospheric models, *Atmos. Chem. Phys.*, 11,
630 4039-4072, <https://doi.org/10.5194/acp-11-4039-2011>, 2011.
- 631
632 Akagi, S. K., Craven, J. S., Taylor, J. W., McMeeking, G. R., Yokelson, R. J., Burling, I. R., Urbanski, S. P., Wold, C.
633 E., Seinfeld, J. H., Coe, H., Alvarado, M. J., and Weise, D. R.: Evolution of trace gases and particles emitted by a
634 chaparral fire in California, *Atmos. Chem. Phys.*, 12, 1397-1421, <https://doi.org/10.5194/acp-12-1397-2012>, 2012.
- 635
636 Akagi, S. K., Burling, I. R., Mendoza, A., Johnson, T. J., Cameron, M., Griffith, D. W. T., Paton-Walsh, C., Weise, D.
637 R., Reardon, J., and Yokelson, R. J.: Field measurements of trace gases emitted by prescribed fires in southeastern US
638 pine forests using an open-path FTIR system, *Atmos. Chem. Phys.*, 14, 199-215, [https://doi.org/10.5194/acp-14-199-](https://doi.org/10.5194/acp-14-199-2014)
639 [2014](https://doi.org/10.5194/acp-14-199-2014), 2014.



- 640
641 Andreae, M. O. and Merlet, P.: Emission of trace gases and aerosols from biomass burning, *Global Biogeochem. Cy.*, 15,
642 955-966, <https://doi.org/10.1029/2000GB001382>, 2001.
- 643
644 Andreae, M. O.: Emission of trace gases and aerosols from biomass burning – an updated assessment, *Atmos. Chem.*
645 *Phys.*, 19, 8523-8546, <https://doi.org/10.5194/acp-19-8523-2019>, 2019.
- 646
647 Apel, E. C., Emmons, L. K., Karl, T., Flocke, F., Hills, A. J., Madronich, S., Lee-Taylor, J., Fried, A., Weibring, P.,
648 Walega, J., Richter, D., Tie, X., Mauldin, L., Campos, T., Weinheimer, A., Knapp, D., Sive, B., Kleinman, L.,
649 Springston, S., Zaveri, R., Ortega, J., Voss, P., Blake, D., Baker, A., Warneke, C., Welsh-Bon, D., de Gouw, J., Zheng,
650 J., Zhang, R., Rudolph, J., Junkermann, W., and Riemer, D. D.: Chemical evolution of volatile organic compounds in the
651 outflow of the Mexico City Metropolitan area, *Atmos. Chem. Phys.*, 10, 2353-2375, [https://doi.org/10.5194/acp-10-](https://doi.org/10.5194/acp-10-2353-2010)
652 [2353-2010](https://doi.org/10.5194/acp-10-2353-2010), 2010.
- 653
654 Apel, E. C., Hornbrook, R. S., Hills, A. J., Blake, N. J., Barth, M. C., Weinheimer, A., Cantrell, C., Rutledge, S. A.,
655 Basarab, B., Crawford, J., Diskin, G., Homeyer, C. R., Campos, T., Flocke, F., Fried, A., Blake, D. R., Brune, W.,
656 Pollack, I., Peischl, J., Ryerson, T., Wennberg, P. O., Crouse, J. D., Wisthaler, A., Mikoviny, T., Huey, G., Heikes, B.,
657 O'Sullivan, D., and Riemer, D. D.: Upper tropospheric ozone production from lightning NO_x-impacted convection:
658 Smoke ingestion case study from the DC3 campaign, *J. Geophys. Res. Atmos.*, 120, 2505-2523,
659 <https://doi.org/10.1002/2014JD022121>, 2015.
- 660
661 Apte, J. S., Brauer, M., Cohen, A. J., Ezzati, M., and Pope, C. A.: Ambient PM_{2.5} Reduces Global and Regional Life
662 Expectancy, *Environ. Sci. Tech. Lett.*, 5, 546-551, <https://doi.org/10.1021/acs.estlett.8b00360>, 2018.
- 663
664 Bond, T. C., Doherty, S. J., Fahey, D. W., Forster, P. M., Berntsen, T., DeAngelo, B. J., Flanner, M. G., Ghan, S.,
665 Kärcher, B., Koch, D., Kinne, S., Kondo, Y., Quinn, P. K., Sarofim, M. C., Schultz, M. G., Schulz, M., Venkataraman,
666 C., Zhang, H., Zhang, S., Bellouin, N., Guttikunda, S. K., Hopke, P. K., Jacobson, M. Z., Kaiser, J. W., Klimont, Z.,
667 Lohmann, U., Schwarz, J. P., Shindell, D., Storelvmo, T., Warren, S. G., and Zender, C. S.: Bounding the role of black
668 carbon in the climate system: A scientific assessment, *J. Geophys. Res. Atmos.*, 118, 5380-5552,
669 <https://doi.org/10.1002/jgrd.50171>, 2013.
- 670
671 Balch, J. K., Bradley, B. A., Abatzoglou, J. T., Nagy, R. C., Fusco, E. J., and Mahood, A. L.: Human-started wildfires
672 expand the fire niche across the United States, *P. Natl. Acad. Sci. USA*, 114, 2946,
673 <https://doi.org/10.1073/pnas.1617394114>, 2017.
- 674
675 Bourgeois, I., Peischl, J., Thompson, C. R., Aikin, K. C., Campos, T., Clark, H., Commane, R., Daube, B., Diskin, G.
676 W., Elkins, J. W., Gao, R. S., Gaudel, A., Hints, E. J., Johnson, B. J., Kivi, R., McKain, K., Moore, F. L., Parrish, D. D.,
677 Querel, R., Ray, E., Sánchez, R., Sweeney, C., Tarasick, D. W., Thompson, A. M., Thouret, V., Witte, J. C., Wofsy, S.
678 C., and Ryerson, T. B.: Global-scale distribution of ozone in the remote troposphere from the ATom and HIPPO airborne
679 field missions, *Atmos. Chem. Phys.*, 20, 10611-10635, <https://doi.org/10.5194/acp-20-10611-2020>, 2020.
- 680
681 Bourgeois, I., Peischl, J., Neuman, J. A., Brown, S. S., Allen, H. M., Campuzano-Jost, P., Coggon, M. M., DiGangi, J.
682 P., Diskin, G. S., Gilman, J. B., Gkatzelis, G. I., Guo, H., Halliday, H. A., Hanisco, T. F., Holmes, C. D., Huey, L. G.,
683 Jimenez, J. L., Lamplugh, A. D., Lee, Y. R., Lindaas, J., Moore, R. H., Nault, B. A., Nowak, J. B., Pagonis, D., Rickly,
684 P. S., Robinson, M. A., Rollins, A. W., Selimovic, V., St. Clair, J. M., Tanner, D., Vasquez, K. T., Veres, P. R.,
685 Warneke, C., Wennberg, P. O., Washenfelder, R. A., Wiggins, E. B., Womack, C. C., Xu, L., Zarzana, K. J., and
686 Ryerson, T. B.: Comparison of airborne measurements of NO, NO₂, HONO, NO_y, and CO during FIREX-AQ, *Atmos.*
687 *Meas. Tech.*, 15, 4901-4930, <https://doi.org/10.5194/amt-15-4901-2022>, 2022.
- 688
689 Braga, R. C., Rosenfeld, D., Weigel, R., Jurkat, T., Andreae, M. O., Wendisch, M., Pöschl, U., Voigt, C., Mahnke, C.,
690 Borrmann, S., Albrecht, R. I., Molleker, S., Vila, D. A., Machado, L. A. T., and Grulich, L.: Further evidence for CCN
691 aerosol concentrations determining the height of warm rain and ice initiation in convective clouds over the Amazon
692 basin, *Atmos. Chem. Phys.*, 17, 14433-14456, <https://doi.org/10.5194/acp-17-14433-2017>, 2017.
- 693
694 Brey, S. J. and Fischer, E. V.: Smoke in the City: How Often and Where Does Smoke Impact Summertime Ozone in the
695 United States? *Environ. Sci. Technol.*, 50, <https://doi.org/10.1021/acs.est.5b05218>, 2015.
- 696
697 Canagaratna, M. R., Jayne, J. T., Jimenez, J. L., Allan, J. D., Alfarra, M. R., Zhang, Q., Onasch, T. B., Drewnick, F.,
698 Coe, H., Middlebrook, A., Delia, A., Williams, L. R., Trimborn, A. M., Northway, M. J., DeCarlo, P. F., Kolb, C. E.,
699 Davidovits, P., and Worsnop, D. R.: Chemical and microphysical characterization of ambient aerosols with the aerodyne
700 aerosol mass spectrometer, *Mass Spectrom. Rev.*, 26, 185-222, <https://doi.org/10.1002/mas.20115>, 2007.



701
702 Cazorla, M., Wolfe, G. M., Bailey, S. A., Swanson, A. K., Arkinson, H. L., and Hanisco, T. F.: A new airborne laser-
703 induced fluorescence instrument for in situ detection of formaldehyde throughout the troposphere and lower stratosphere,
704 *Atmos. Meas. Tech.*, 8, 541–552, <https://doi.org/10.5194/amt-8-541-2015>, 2015.
705
706 Cecchini, M. A., Machado, L. A. T., Andreae, M. O., Martin, S. T., Albrecht, R. I., Artaxo, P., Barbosa, H. M. J.,
707 Borrmann, S., Fütterer, D., Jurkat, T., Mahnke, C., Minikin, A., Molleker, S., Pöhlker, M. L., Pöschl, U., Rosenfeld, D.,
708 Voigt, C., Weinzierl, B., and Wendisch, M.: Sensitivities of Amazonian clouds to aerosols and updraft speed, *Atmos.*
709 *Chem. Phys.*, 17, <https://doi.org/10037-10050>, <https://doi.org/10.5194/acp-17-10037-2017>, 2017.
710
711 Cochrane, M. A., Moran, C. J., Wimberly, M. C., Baer, A. D., Finney, M. A., Beckendorf, K. L., Eidenshink, J., and
712 Zhu, Z.: Estimation of wildfire size and risk changes due to fuels treatments, *Int. J. Wildland Fire*, 21, 357–367,
713 <https://doi.org/10.1071/WF11079>, 2012.
714
715 Coggon, M. M., Lim, C. Y., Koss, A. R., Sekimoto, K., Yuan, B., Gilman, J. B., Hagan, D. H., Selimovic, V., Zarzana,
716 K. J., Brown, S. S., Roberts, J. M., Müller, M., Yokelson, R., Wisthaler, A., Krechmer, J. E., Jimenez, J. L., Cappa, C.,
717 Kroll, J. H., de Gouw, J., and Warneke, C.: OH chemistry of non-methane organic gases (NMOGs) emitted from
718 laboratory and ambient biomass burning smoke: evaluating the influence of furans and oxygenated aromatics on ozone
719 and secondary NMOG formation, *Atmos. Chem. Phys.*, 19, 14875–14899, <https://doi.org/10.5194/acp-19-14875-2019>,
720 2019.
721
722 Colman, J. J., Swanson, A. L., Meinardi, S., Sive, B. C., Blake, D. R., and Rowland, F. S.: Description of the Analysis of
723 a Wide Range of Volatile Organic Compounds in Whole Air Samples Collected during PEM-Tropics A and B, *Anal.*
724 *Chem.*, 73, 3723–3731, <https://doi.org/10.1021/ac010027g>, 2001.
725
726 Crouse, J. D., McKinney, K. A., Kwan, A. J., and Wennberg, P. O.: Measurement of Gas-Phase Hydroperoxides by
727 Chemical Ionization Mass Spectrometry, *Anal. Chem.*, 78, 6726–6732, <https://doi.org/10.1021/ac0604235>, 2006.
728
729 Crutzen, P. J. and Andreae, M. O.: Biomass Burning in the Tropics: Impact on Atmospheric Chemistry and
730 Biogeochemical Cycles, *Science*, 250, 1669, <https://doi.org/10.1126/science.250.4988.1669>, 1990.
731
732 Day, D. A., Campuzano-Jost, P., Nault, B. A., Palm, B. B., Hu, W., Guo, H., Wooldridge, P. J., Cohen, R. C., Docherty,
733 K. S., Huffman, J. A., de Sá, S. S., Martin, S. T., and Jimenez, J. L.: A Systematic Re-evaluation of Methods for
734 Quantification of Bulk Particle-phase Organic Nitrates Using Real-time Aerosol Mass Spectrometry, *Atmos. Meas.*
735 *Tech.*, 15, 459–483, <https://doi.org/10.5194/amt-15-459-2022>, 2022.
736
737 Decker, Z. C. J., Robinson, M. A., Barsanti, K. C., Bourgeois, I., Coggon, M. M., DiGangi, J. P., Diskin, G. S., Flocke,
738 F. M., Franchin, A., Fredrickson, C. D., Hall, S. R., Halliday, H., Holmes, C. D., Huey, L. G., Lee, Y. R., Lindaas, J.,
739 Middlebrook, A. M., Montzka, D. D., Moore, R. H., Neuman, J. A., Nowak, J. B., Palm, B. B., Peischl, J., Piel, F.,
740 Rickly, P. S., Rollins, A. W., Ryerson, T. B., Schwantes, R. H., Sekimoto, K., Thornhill, L., Thornton, J. A., Tyndall, G.
741 S., Ullmann, K., Van Rooy, P., Veres, P. R., Warneke, C., Washenfelder, R. A., Weinheimer, A. J., Wiggins, E.,
742 Winstead, E., Wisthaler, A., Womack, C., and Brown, S. S.: Nighttime and daytime dark oxidation chemistry in wildfire
743 plumes: an observation and model analysis of FIREX-AQ aircraft data, *Atmos. Chem. Phys.*, 21, 16293–16317,
744 <https://doi.org/10.5194/acp-21-16293-2021>, 2021.
745
746 Dennekamp, M., Straney, L. D., Erbas, B., Abramson, M. J., Keywood, M., Smith, K., Sim, M. R., Glass, D. C., Del
747 Monaco, A., Haikerwal, A., and Tonkin, A. M.: Forest Fire Smoke Exposures and Out-of-Hospital Cardiac Arrests in
748 Melbourne, Australia: A Case-Crossover Study, *Environ. Health Persp.*, 123, 959–964,
749 <https://doi.org/10.1289/ehp.1408436>, 2015.
750
751 Finewax, Z., de Gouw, J. A., and Ziemann, P. J.: Identification and Quantification of 4-Nitrocatechol Formed from OH
752 and NO₃ Radical-Initiated Reactions of Catechol in Air in the Presence of NO_x: Implications for Secondary Organic
753 Aerosol Formation from Biomass Burning, *Environ. Sci. Technol.*, 52, 1981–1989,
754 <https://doi.org/10.1021/acs.est.7b05864>, 2018.
755
756 Flannigan, M., Cantin, A. S., de Groot, W. J., Wotton, M., Newbery, A., and Gowman, L. M.: Global wildland fire
757 season severity in the 21st century, *For. Ecol. Manag.*, 294, 54–61, <https://doi.org/10.1016/j.foreco.2012.10.022>, 2013.
758
759 Fried, A., et al.: Airborne formaldehyde and volatile organic compound measurements over the Daesan petrochemical
760 complex on Korea's northwest coast during the Korea-United States Air Quality study: Estimation of emission fluxes
761 and effects on air quality, *Elem Sci Anth*, 8:1, <https://doi.org/10.1525/elementa.2020.121>, 2020.



762
763 Gilman, J. B., Lerner, B. M., Kuster, W. C., Goldan, P. D., Warneke, C., Veres, P. R., Roberts, J. M., de Gouw, J. A.,
764 Burling, I. R., and Yokelson, R. J.: Biomass burning emissions and potential air quality impacts of volatile organic
765 compounds and other trace gases from fuels common in the US, *Atmos. Chem. Phys.*, 15, 13915-13938,
766 <https://doi.org/10.5194/acp-15-13915-2015>, 2015.
767
768 Griffin, D., McLinden, C. A., Dammers, E., Adams, C., Stockwell, C. E., Warneke, C., Bourgeois, I., Peischl, J.,
769 Ryerson, T. B., Zarzana, K. J., Rowe, J. P., Volkamer, R., Knote, C., Kille, N., Koenig, T. K., Lee, C. F., Rollins, D.,
770 Rickly, P. S., Chen, J., Fehr, L., Bourassa, A., Degenstein, D., Hayden, K., Mihele, C., Wren, S. N., Liggio, J.,
771 Akingunola, A., and Makar, P.: Biomass burning nitrogen dioxide emissions derived from space with TROPOMI:
772 methodology and validation, *Atmos. Meas. Tech.*, 14, 7929-7957, <https://doi.org/10.5194/amt-14-7929-2021>, 2021.
773
774 Guo, H., Campuzano-Jost, P., Nault, B. A., Day, D. A., Schroder, J. C., Kim, D., Dibb, J. E., Dollner, M., Weinzierl, B.,
775 and Jimenez, J. L.: The importance of size ranges in aerosol instrument intercomparisons: a case study for the
776 Atmospheric Tomography Mission, *Atmos. Meas. Tech.*, 14, 3631-3655, <https://doi.org/10.5194/amt-14-3631-2021>,
777 2021.
778
779 Hamilton, D. S., Hantson, S., Scott, C. E., Kaplan, J. O., Pringle, K. J., Nieradzik, L. P., Rap, A., Folberth, G. A.,
780 Spracklen, D. V., and Carslaw, K. S.: Reassessment of pre-industrial fire emissions strongly affects anthropogenic
781 aerosol forcing, *Nat. Commun.*, 9, 3182, <https://doi.org/10.1038/s41467-018-05592-9>, 2018.
782
783 Hatch, L. E., Yokelson, R. J., Stockwell, C. E., Veres, P. R., Simpson, I. J., Blake, D. R., Orlando, J. J., and Barsanti, K.
784 C.: Multi-instrument comparison and compilation of non-methane organic gas emissions from biomass burning and
785 implications for smoke-derived secondary organic aerosol precursors, *Atmos. Chem. Phys.*, 17, 1471-1489,
786 <https://doi.org/10.5194/acp-17-1471-2017>, 2017.
787
788 Hodshire, A. L., Bian, Q., Ramnarine, E., Lonsdale, C. R., Alvarado, M. J., Kreidenweis, S. M., Jathar, S. H., and Pierce,
789 J. R.: More Than Emissions and Chemistry: Fire Size, Dilution, and Background Aerosol Also Greatly Influence Near-
790 Field Biomass Burning Aerosol Aging, *J. Geophys. Res. Atmos.*, 124, 5589-5611,
791 <https://doi.org/10.1029/2018JD029674>, 2019.
792
793 Holder, A. L., Gullett, B. K., Urbanski, S. P., Elleman, R., O'Neill, S., Tabor, D., Mitchell, W., and Baker, K. R.:
794 Emissions from prescribed burning of agricultural fields in the Pacific Northwest, *Atmos. Environ.*, 166, 22-33,
795 <https://doi.org/10.1016/j.atmosenv.2017.06.043>, 2017.
796
797 Holmes, C. D., Fite, C., Agastra, A., Schwarz, J. P., Yokelson, R. J., Bui, T. V., and Peterson, D. A.: Critical evaluation
798 of smoke age inferred from different methods during FIREX-AQ,
799 <https://ui.adsabs.harvard.edu/abs/2020AGUFMA225.0010H>, 2020.
800
801 Isaacman-VanWertz, G., Sueper, D. T., Aikin, K. C., Lerner, B. M., Gilman, J. B., de Gouw, J. A., Worsnop, D. R., and
802 Goldstein, A. H.: Automated single-ion peak fitting as an efficient approach for analyzing complex chromatographic
803 data, *J. Chromatogr. A*, 1529, 81-92, <https://doi.org/10.1016/j.chroma.2017.11.005>, 2017.
804
805 Johnston, F. H., Henderson, S. B., Chen, Y., Randerson, J. T., Marlier, M., DeFries, R. S., Kinney, P., Bowman, D. M. J.
806 S., and Brauer, M.: Estimated Global Mortality Attributable to Smoke from Landscape Fires, *Environ. Health Persp.*,
807 120, 695-701, <https://doi.org/10.1289/ehp.1104422>, 2012.
808
809 Jung, Y., González Abad, G., Nowlan, C. R., Chance, K., Liu, X., Torres, O., and Ahn, C.: Explicit Aerosol Correction
810 of OMI Formaldehyde Retrievals, *Earth and Space Science*, 6, 2087-2105, <https://doi.org/10.1029/2019EA000702>, 2019.
811
812 Keywood, M., Kanakidou, M., Stohl, A., Dentener, F., Grassi, G., Meyer, C. P., Torseth, K., Edwards, D., Thompson, A.
813 M., Lohmann, U., and Burrows, J.: Fire in the Air: Biomass Burning Impacts in a Changing Climate, *Crit. Rev. i Environ.*
814 *Sci. Technol.*, 43, 40-83, <https://doi.org/10.1080/10643389.2011.604248>, 2013.
815
816 Kloster, S., Mahowald, N. M., Randerson, J. T., Thornton, P. E., Hoffman, F. M., Levis, S., Lawrence, P. J., Feddema, J.
817 J., Oleson, K. W., and Lawrence, D. M.: Fire dynamics during the 20th century simulated by the Community Land
818 Model, *Biogeosciences*, 7, 1877-1902, <https://doi.org/10.5194/bg-7-1877-2010>, 2010.
819
820 Knorr, W., Dentener, F., Lamarque, J. F., Jiang, L., and Armeth, A.: Wildfire air pollution hazard during the 21st century,
821 *Atmos. Chem. Phys.*, 17, 9223-9236, <https://doi.org/10.5194/acp-17-9223-2017>, 2017.
822



823 Kodros, J. K., Papanastasiou, D. K., Paglione, M., Masiol, M., Squizzato, S., Florou, K., Skyllakou, K., Kaltsonoudis, C.,
824 Nenes, A., and Pandis, S. N.: Rapid dark aging of biomass burning as an overlooked source of oxidized organic aerosol,
825 *P. Natl. Acad. Sci. USA*, 117, 33028, <https://doi.org/10.1073/pnas.2010365117>, 2020.
826
827 Kononov, I. B., Lvova, D. A., Beekmann, M., Jethva, H., Mikhailov, E. F., Paris, J. D., Belan, B. D., Kozlov, V. S.,
828 Ciais, P., and Andreae, M. O.: Estimation of black carbon emissions from Siberian fires using satellite observations of
829 absorption and extinction optical depths, *Atmos. Chem. Phys.*, 18, 14889-14924, [https://doi.org/10.5194/acp-18-14889-](https://doi.org/10.5194/acp-18-14889-2018)
830 [2018](https://doi.org/10.5194/acp-18-14889-2018), 2018.
831
832 Koss, A. R., Sekimoto, K., Gilman, J. B., Selimovic, V., Coggon, M. M., Zarzana, K. J., Yuan, B., Lerner, B. M., Brown,
833 S. S., Jimenez, J. L., Krechmer, J., Roberts, J. M., Warneke, C., Yokelson, R. J., and de Gouw, J.: Non-methane organic
834 gas emissions from biomass burning: identification, quantification, and emission factors from PTR-ToF during the
835 FIREX 2016 laboratory experiment, *Atmos. Chem. Phys.*, 18, 3299-3319, <https://doi.org/10.5194/acp-18-3299-2018>,
836 2018.
837
838 Le Quéré, C., Andrew, R. M., Friedlingstein, P., Sitch, S., Hauck, J., Pongratz, J., Pickers, P. A., Korsbakken, J. I.,
839 Peters, G. P., Canadell, J. G., Armeth, A., Arora, V. K., Barbero, L., Bastos, A., Bopp, L., Chevallier, F., Chini, L. P.,
840 Ciais, P., Doney, S. C., Gkritzalis, T., Goll, D. S., Harris, I., Haverd, V., Hoffman, F. M., Hoppema, M., Houghton, R.
841 A., Hurtt, G., Ilyina, T., Jain, A. K., Johannessen, T., Jones, C. D., Kato, E., Keeling, R. F., Goldewijk, K. K.,
842 Landschützer, P., Lefèvre, N., Lienert, S., Liu, Z., Lombardozi, D., Metz, N., Munro, D. R., Nabel, J. E. M. S.,
843 Nakaoka, S., Neill, C., Olsen, A., Ono, T., Patra, P., Peregón, A., Peters, W., Peylin, P., Pfeil, B., Pierrot, D., Poulter, B.,
844 Rehder, G., Resplandy, L., Robertson, E., Rocher, M., Rödenbeck, C., Schuster, U., Schwinger, J., Séférian, R.,
845 Skjelvan, I., Steinhoff, T., Sutton, A., Tans, P. P., Tian, H., Tilbrook, B., Tubiello, F. N., van der Laan-Luijckx, I. T., van
846 der Werf, G. R., Viovy, N., Walker, A. P., Wiltshire, A. J., Wright, R., Zaehle, S., and Zheng, B.: Global Carbon Budget
847 2018, *Earth Syst. Sci. Data*, 10, 2141-2194, <https://doi.org/10.5194/essd-10-2141-2018>, 2018.
848
849 Lerner, B. M., Gilman, J. B., Aikin, K. C., Atlas, E. L., Goldan, P. D., Graus, M., Hendershot, R., Isaacman-VanWertz,
850 G. A., Koss, A., Kuster, W. C., Lueb, R. A., McLaughlin, R. J., Peischl, J., Sueper, D., Ryerson, T. B., Tokarek, T. W.,
851 Warneke, C., Yuan, B., and de Gouw, J. A.: An improved, automated whole air sampler and gas chromatography mass
852 spectrometry analysis system for volatile organic compounds in the atmosphere, *Atmos. Meas. Tech.*, 10, 291-313,
853 <https://doi.org/10.5194/amt-10-291-2017>, 2017.
854
855 Liao, J., Wolfe, G. M., Hannun, R. A., St. Clair, J. M., Hanisco, T. F., Gilman, J. B., Lamplugh, A., Selimovic, V.,
856 Diskin, G. S., Nowak, J. B., Halliday, H. S., DiGangi, J. P., Hall, S. R., Ullmann, K., Holmes, C. D., Fite, C. H., Agastra,
857 A., Ryerson, T. B., Peischl, J., Bourgeois, I., Warneke, C., Coggon, M. M., Gkatzelis, G. I., Sekimoto, K., Fried, A.,
858 Richter, D., Weibring, P., Apel, E. C., Hornbrook, R. S., Brown, S. S., Womack, C. C., Robinson, M. A., Washenfelder,
859 R. A., Veres, P. R., and Neuman, J. A.: Formaldehyde evolution in U.S. wildfire plumes during the Fire Influence on
860 Regional to Global Environments and Air Quality experiment (FIREX-AQ), *Atmos. Chem. Phys.*, 21, 18319-18331,
861 <https://doi.org/10.5194/acp-21-18319-2021>, 2021.
862
863 Lindaas, J., Pollack, I. B., Garofalo, L. A., Pothier, M. A., Farmer, D. K., Kreidenweis, S. M., Campos, T. L., Flocke, F.,
864 Weinheimer, A. J., Montzka, D. D., Tyndall, G. S., Palm, B. B., Peng, Q., Thornton, J. A., Permar, W., Wielgasz, C., Hu,
865 L., Ottmar, R. D., Restaino, J. C., Hudak, A. T., Ku, I. T., Zhou, Y., Sive, B. C., Sullivan, A., Collett Jr, J. L., and
866 Fischer, E. V.: Emissions of Reactive Nitrogen From Western U.S. Wildfires During Summer 2018, *J. Geophys. Res.*
867 *Atmos.*, 126, e2020JD032657, <https://doi.org/10.1029/2020JD032657>, 2021.
868
869 Ling, Z., Xie, Q., Shao, M., Wang, Z., Wang, T., Guo, H., and Wang, X.: Formation and sink of glyoxal and
870 methylglyoxal in a polluted subtropical environment: observation-based photochemical analysis and impact evaluation,
871 *Atmos. Chem. Phys.*, 20, 11451-11467, <https://doi.org/10.5194/acp-20-11451-2020>, 2020.
872
873 Liu, X., Huey, L. G., Yokelson, R. J., Selimovic, V., Simpson, I. J., Müller, M., Jimenez, J. L., Campuzano-Jost, P.,
874 Beyersdorf, A. J., Blake, D. R., Butterfield, Z., Choi, Y., Crouse, J. D., Day, D. A., Diskin, G. S., Dubey, M. K.,
875 Fortner, E., Hanisco, T. F., Hu, W., King, L. E., Kleinman, L., Meinardi, S., Mikoviny, T., Onasch, T. B., Palm, B. B.,
876 Peischl, J., Pollack, I. B., Ryerson, T. B., Sachse, G. W., Sedlacek, A. J., Shilling, J. E., Springston, S., St. Clair, J. M.,
877 Tanner, D. J., Teng, A. P., Wennberg, P. O., Wisthaler, A., and Wolfe, G. M.: Airborne measurements of western U.S.
878 wildfire emissions: Comparison with prescribed burning and air quality implications, *J. Geophys. Res. Atmos.*, 122,
879 6108-6129, <https://doi.org/10.1002/2016JD026315>, 2017.
880
881 Mann, M. L., Batllori, E., Moritz, M. A., Waller, E. K., Berck, P., Flint, A. L., Flint, L. E., and Dolfi, E.: Incorporating
882 Anthropogenic Influences into Fire Probability Models: Effects of Human Activity and Climate Change on Fire Activity
883 in California, *PLOS ONE*, 11, e0153589, <https://doi.org/10.1371/journal.pone.0153589>, 2016.



884
885 Martínez-Alonso, S., Deeter, M., Worden, H., Borsdorff, T., Aben, I., Commane, R., Daube, B., Francis, G., George, M.,
886 Landgraf, J., Mao, D., McKain, K., and Wofsy, S.: 1.5 years of TROPOMI CO measurements: comparisons to MOPITT
887 and ATom, *Atmos. Meas. Tech.*, 13, 4841–4864, <https://doi.org/10.5194/amt-13-4841-2020>, 2020.
888
889 Min, K. E., Washenfelder, R. A., Dubé, W. P., Langford, A. O., Edwards, P. M., Zarzana, K. J., Stutz, J., Lu, K., Rohrer,
890 F., Zhang, Y., and Brown, S. S.: A broadband cavity enhanced absorption spectrometer for aircraft measurements of
891 glyoxal, methylglyoxal, nitrous acid, nitrogen dioxide, and water vapor, *Atmos. Meas. Tech.*, 9, 423–440,
892 <https://doi.org/10.5194/amt-9-423-2016>, 2016.
893
894 Mitsuishi, K., Iwasaki, M., Takeuchi, M., Okochi, H., Kato, S., Ohira, S.-I., and Toda, K.: Diurnal Variations in
895 Partitioning of Atmospheric Glyoxal and Methylglyoxal between Gas and Particles at the Ground Level and in the Free
896 Troposphere, *ACS Earth Space Chem.*, 2, 915–924, <https://doi.org/10.1021/acsearthspacechem.8b00037>, 2018.
897
898 Moritz, M. A., Parisien, M.-A., Battlori, E., Krawchuk, M. A., Van Dorn, J., Ganz, D. J., and Hayhoe, K.: Climate
899 change and disruptions to global fire activity, *Ecosphere*, 3, 49, <https://doi.org/10.1890/ES11-00345.1>, 2012.
900
901 Mouat, A. P., Paton-Walsh, C., Simmons, J. B., Ramirez-Gamboa, J., Griffith, D. W. T., and Kaiser, J.: Emission factors
902 of long-lived volatile organic compounds from the 2019–2020 Australian wildfires during the COALA campaign, *Atmos.*
903 *Chem. Phys. Discuss.*, 2021, 1–13, <https://doi.org/10.5194/acp-2021-742>, 2021.
904
905 Müller, M., Anderson, B. E., Beyersdorf, A. J., Crawford, J. H., Diskin, G. S., Eichler, P., Fried, A., Keutsch, F. N.,
906 Mikoviny, T., Thornhill, K. L., Walega, J. G., Weinheimer, A. J., Yang, M., Yokelson, R. J., and Wisthaler, A.: In situ
907 measurements and modeling of reactive trace gases in a small biomass burning plume, *Atmos. Chem. Phys.*, 16, 3813–
908 3824, <https://doi.org/10.5194/acp-16-3813-2016>, 2016.
909
910 NASA airborne science data for atmospheric composition, <https://doi.org/10.5067/suborbital/firexaq2019/data001>, 2019.
911
912 National Interagency Fire Center; Internetseite vom 24.10.2015: Total Wildland Fires and Acres (1960–2009).
913 http://www.nifc.gov/fireInfo/fireInfo_stats_totalFires.html, <https://www.nifc.gov/fire-information/statistics/wildfires>,
914 <https://www.nifc.gov/fire-information/statistics/prescribed-fire>
915
916 Olivier, J. G. J., Van Aardenne, J. A., Dentener, F. J., Pagliari, V., Ganzeveld, L. N., and Peters, J. A. H. W.: Recent
917 trends in global greenhouse gas emissions: regional trends 1970–2000 and spatial distribution of key sources in 2000,
918 *Environmental Sciences*, 2, 81–99, <https://doi.org/10.1080/15693430500400345>, 2005.
919
920 Pagonis, D., Sekimoto, K. and de Gouw, J. A.: A library of proton-transfer reactions of H₃O⁺ ions used for trace gas
921 detection, *J. Am. Soc. Mass Spectrom.*, 30, 1330–1335, <https://doi.org/10.1007/s13361-019-02209-3>, 2019.
922
923 Pagonis, D., Campuzano-Jost, P., Guo, H., Day, D. A., Schueneman, M., Nault, B. A., Brown, W., Laskin, A., Siemens,
924 K. S. A., Coggon, M. M., DiGangi, J. P., Diskin, G. S., Fenn, M. A., Gkatzelis, G., Hair, J. W., Halliday, H. S., Katich, J.
925 M., Nowak, J. B., Perring, A. E., Saide, P. E., Sekimoto, K., Shingler, T. J., Thapa, L., Warneke, C., and Jimenez, J. L.:
926 Chemical Aging of Biomass Burning Organic Aerosol: Insight from Fast Near-Molecular Measurements, December 01,
927 2020.
928
929 Pagonis, D., Campuzano-Jost, P., Guo, H., Day, D. A., Schueneman, M. K., Brown, W. L., Nault, B. A., Stark, H.,
930 Siemens, K., Laskin, A., Piel, F., Tomsche, L., Wisthaler, A., Coggon, M. M., Gkatzelis, G. I., Halliday, H. S.,
931 Krechmer, J. E., Moore, R. H., Thomson, D. S., Warneke, C., Wiggins, E. B., and Jimenez, J. L.: Airborne extractive
932 electrospray mass spectrometry measurements of the chemical composition of organic aerosol, *Atmos. Meas. Tech.*, 14,
933 1545–1559, <https://doi.org/10.5194/amt-14-1545-2021>, 2021.
934
935 Pechony, O. and Shindell, D. T.: Driving forces of global wildfires over the past millennium and the forthcoming
936 century, *P. Natl. Acad. Sci. USA*, 107, 19167, <https://doi.org/10.1073/pnas.1003669107>, 2010.
937
938 Peng, Q., Palm, B. B., Melander, K. E., Lee, B. H., Hall, S. R., Ullmann, K., Campos, T., Weinheimer, A. J., Apel, E. C.,
939 Hornbrook, R. S., Hills, A. J., Montzka, D. D., Flocke, F., Hu, L., Permar, W., Wielgasz, C., Lindaas, J., Pollack, I. B.,
940 Fischer, E. V., Bertram, T. H., and Thornton, J. A.: HONO Emissions from Western U.S. Wildfires Provide Dominant
941 Radical Source in Fresh Wildfire Smoke, *Environ. Sci. Technol.*, 54, 5954–5963,
942 <https://doi.org/10.1021/acs.est.0c00126>, 2020.
943



- 944 Permar, W., Wang, Q., Selimovic, V., Wielgasz, C., Yokelson, R. J., Hornbrook, R. S., Hills, A. J., Apel, E. C., Ku, I. T.,
945 Zhou, Y., Sive, B. C., Sullivan, A. P., Collett Jr, J. L., Campos, T. L., Palm, B. B., Peng, Q., Thornton, J. A., Garofalo,
946 L. A., Farmer, D. K., Kreidenweis, S. M., Levin, E. J. T., DeMott, P. J., Flocke, F., Fischer, E. V., and Hu, L.: Emissions
947 of Trace Organic Gases From Western U.S. Wildfires Based on WE-CAN Aircraft Measurements, *J. Geophys. Res.*
948 *Atmos.*, 126, e2020JD033838, <https://doi.org/10.1029/2020JD033838>, 2021.
- 949
950 Prichard, S. J., O'Neill, S. M., Eagle, P., Andreu, A. G., Drye, B., Dubowy, J., Urbanski, S., and Strand, T. M.: Wildland
951 fire emission factors in North America: synthesis of existing data, measurement needs and management applications, *Int.*
952 *J. Wildland Fire*, 29, 132-147, <https://doi.org/10.1071/WF19066>, 2020.
- 953
954 Reddington, C. L., Spracklen, D. V., Artaxo, P., Ridley, D. A., Rizzo, L. V., and Arana, A.: Analysis of particulate
955 emissions from tropical biomass burning using a global aerosol model and long-term surface observations, *Atmos.*
956 *Chem. Phys.*, 16, 11083-11106, <https://doi.org/10.5194/acp-16-11083-2016>, 2016.
- 957
958 Richter, D., Weibring, P., Walega, J.G., Fried, A., Spuler, S.M., and Taubman, M.S.: Compact highly sensitive multi-
959 species airborne mid-IR spectrometer, *Appl. Phys. B.*, <https://doi.org/10.1007/s00340-015-6038-8>, 2015.
- 960
961 Rickly, P., Guo, H., Campuzano-Jost, P., Jimenez, J. L., Wolfe, G. M., Bennett, R., Bourgeois, I., Crouse, J. D., Dibb, J.
962 E., DiGangi, J. P., Diskin, G. S., Dollner, M., Gargulinski, E. M., Hall, S. R., Halliday, H. S., Hanisco, T. F., Hannun, R.
963 A., Liao, J., Moore, R., Nault, B. A., Nowak, J. B., Robinson, C. E., Ryerson, T., Sanchez, K. J., Schöberl, M., Soja, A.
964 J., St. Clair, J. M., Thornhill, K. L., Ullmann, K., Wennberg, P. O., Weinzierl, B., Wiggins, E. B., Winstead, E. L., and
965 Rollins, A. W.: Emission factors and evolution of SO₂ measured from biomass burning in wild and agricultural fires,
966 *Atmos. Chem. Phys. Discuss.*, 2022, 1-29, <https://doi.org/10.5194/acp-2022-309>, 2022.
- 967
968 Roberts, J. M., Stockwell, C. E., Yokelson, R. J., de Gouw, J., Liu, Y., Selimovic, V., Koss, A. R., Sekimoto, K.,
969 Coggon, M. M., Yuan, B., Zarzana, K. J., Brown, S. S., Santin, C., Doerr, S. H., and Warneke, C.: The nitrogen budget
970 of laboratory-simulated western US wildfires during the FIREX 2016 Fire Lab study, *Atmos. Chem. Phys.*, 20, 8807-
971 8826, <https://doi.org/10.5194/acp-20-8807-2020>, 2020.
- 972
973 Robinson, M. A., Decker, Z. C. J., Barsanti, K. C., Coggon, M. M., Flocke, F. M., Franchin, A., Fredrickson, C. D.,
974 Gilman, J. B., Gkatzelis, G. I., Holmes, C. D., Lamplugh, A., Lavi, A., Middlebrook, A. M., Montzka, D. M., Palm, B.
975 B., Peischl, J., Pierce, B., Schwantes, R. H., Sekimoto, K., Selimovic, V., Tyndall, G. S., Thornton, J. A., Van Rooy, P.,
976 Warneke, C., Weinheimer, A. J., and Brown, S. S.: Variability and Time of Day Dependence of Ozone Photochemistry
977 in Western Wildfire Plumes, *Environ. Sci. Technol.*, 55, 10280-10290, <https://doi.org/10.1021/acs.est.1c01963>, 2021.
- 978
979 Rollins, A. W., Rickly, P. S., Gao, R. S., Ryerson, T. B., Brown, S. S., Peischl, J., and Bourgeois, I.: Single-photon laser-
980 induced fluorescence detection of nitric oxide at sub-parts-per-trillion mixing ratios, *Atmos. Meas. Tech.*, 13, 2425-2439,
981 <https://doi.org/10.5194/amt-13-2425-2020>, 2020.
- 982
983 Ryerson, T. B., Williams, E. J., and Fehsenfeld, F. C.: An efficient photolysis system for fast-response NO₂
984 measurements, *Journal of Geophysical Research: Atmospheres*, 105, 26447-26461,
985 <https://doi.org/10.1029/2000JD900389>, 2000.
- 986
987 Sachse, G. W., Collins, J., Hill, G. F., Wade, L. O., Burney, L. G., and Ritter, J. A.: Airborne tunable diode laser sensor
988 for high-precision concentration and flux measurements of carbon monoxide and methane, *Photonics West - Lasers and*
989 *Applications in Science and Engineering*, <https://doi.org/10.1117/12.46162>, 1991.
- 990
991 Sachse, S. W., Collins, J. E., Hill, G. F., Wade, L. O., Burney, L. G., and Ritter, J. A.: Airborne tunable diode laser
992 sensor for high-precision concentration and flux measurements of carbon monoxide and methane, *Proc.SPIE*, 1991.
- 993 Schwarz, J. P., Gao, R. S., Spackman, J. R., Watts, L. A., Thomson, D. S., Fahey, D. W., Ryerson, T. B., Peischl, J.,
994 Holloway, J. S., Trainer, M., Frost, G. J., Baynard, T., Lack, D. A., de Gouw, J. A., Warneke, C., and Del Negro, L. A.:
995 Measurement of the mixing state, mass, and optical size of individual black carbon particles in urban and biomass
996 burning emissions, *Geophys. Res. Lett.*, 35, L13810, <https://doi.org/10.1029/2008gl033968>, 2008.
- 997
998 Schneising, O., Buchwitz, M., Reuter, M., Bovensmann, H., and Burrows, J. P.: Severe Californian wildfires in
999 November 2018 observed from space: the carbon monoxide perspective, *Atmos. Chem. Phys.*, 20, 3317-3332,
1000 <https://doi.org/10.5194/acp-20-3317-2020>, 2020.
- 1001
1002 Schwarz, J. P., Spackman, J. R., Fahey, D. W., Gao, R. S., Lohmann, U., Stier, P., Watts, L. A., Thomson, D. S., Lack,
1003 D. A., Pfister, L., Mahoney, M. J., Baumgardner, D., Wilson, J. C., and Reeves, J. M.: Coatings and their enhancement



- 1004 of black carbon light absorption in the tropical atmosphere, *J. Geophys. Res. Atmos.*, 113, D03203,
1005 <https://doi.org/10.1029/2007JD009042>, 2008.
- 1006
- 1007 Sekimoto, K., Li, S.-M., Yuan, B., Koss, A., Coggon, M., Warneke, C., and de Gouw, J.: Calculation of the sensitivity of
1008 proton-transfer-reaction mass spectrometry (PTR-MS) for organic trace gases using molecular properties, *Int. J. Mass*
1009 *Spectrom.*, 421, 71-94, <https://doi.org/10.1016/j.ijms.2017.04.006>, 2017.
- 1010
- 1011 Sekimoto, K., Koss, A. R., Gilman, J. B., Selimovic, V., Coggon, M. M., Zarzana, K. J., Yuan, B., Lerner, B. M., Brown,
1012 S. S., Warneke, C., Yokelson, R. J., Roberts, J. M., and de Gouw, J.: High- and low-temperature pyrolysis profiles
1013 describe volatile organic compound emissions from western US wildfire fuels, *Atmos. Chem. Phys.*, 18, 9263-9281,
1014 <https://doi.org/10.5194/acp-18-9263-2018>, 2018.
- 1015
- 1016 Selimovic, V., Yokelson, R. J., Warneke, C., Roberts, J. M., de Gouw, J., Reardon, J., and Griffith, D. W. T.: Aerosol
1017 optical properties and trace gas emissions by PAX and OP-FTIR for laboratory-simulated western US wildfires during
1018 FIREX, *Atmos. Chem. Phys.*, 18, 2929-2948, <https://doi.org/10.5194/acp-18-2929-2018>, 2018.
- 1019
- 1020 Shrivastava, M., Cappa, C. D., Fan, J., Goldstein, A. H., Guenther, A. B., Jimenez, J. L., Kuang, C., Laskin, A., Martin,
1021 S. T., Ng, N. L., Petaja, T., Pierce, J. R., Rasch, P. J., Roldin, P., Seinfeld, J. H., Shilling, J., Smith, J. N., Thornton, J. A.,
1022 Volkamer, R., Wang, J., Worsnop, D. R., Zaveri, R. A., Zelenyuk, A., and Zhang, Q.: Recent advances in understanding
1023 secondary organic aerosol: Implications for global climate forcing, *Rev. Geophys.*, 55, 509-559,
1024 <https://doi.org/10.1002/2016RG000540>, 2017.
- 1025
- 1026 Simpson, I. J., Colman, J. J., Swanson, A. L., Bandy, A. R., Thornton, D. C., Blake, D. R., and Rowland, F. S.: Aircraft
1027 Measurements of Dimethyl Sulfide (DMS) Using a Whole Air Sampling Technique, *J. Atmos. Chem.*, 39, 191-213,
1028 <https://doi.org/10.1023/A:1010608529779>, 2001.
- 1029
- 1030 Simpson, I. J., Blake, D. R., Blake, N. J., Meinardi, S., Barletta, B., Hughes, S. C., Fleming, L. T., Crawford, J. H.,
1031 Diskin, G. S., Emmons, L. K., Fried, A., Guo, H., Peterson, D. A., Wisthaler, A., Woo, J.-H., Barré, J., Gaubert, B., Kim,
1032 J., Kim, M. J., Kim, Y., Knote, C., Mikoviny, T., Pusede, S. E., Schroeder, J. R., Wang, Y., Wennberg, P. O., and Zeng,
1033 L.: Characterization, sources and reactivity of volatile organic compounds (VOCs) in Seoul and surrounding regions
1034 during KORUS-AQ, *Elementa: Science of the Anthropocene*, 8, <https://doi.org/10.1525/elementa.434>, 2020.
- 1035
- 1036 Spracklen, D. V., Mickley, L. J., Logan, J. A., Hudman, R. C., Yevich, R., Flannigan, M. D., and Westerling, A. L.:
1037 Impacts of climate change from 2000 to 2050 on wildfire activity and carbonaceous aerosol concentrations in the
1038 western United States, *J. Geophys. Res. Atmos.*, 114, <https://doi.org/10.1029/2008JD010966>, 2009.
- 1039
- 1040 Stark, H., Yatavelli, R. L. N., Thompson, S. L., Kimmel, J. R., Cubison, M. J., Chhabra, P. S., Canagaratna, M. R.,
1041 Jayne, J. T., Worsnop, D. R., and Jimenez, J. L.: Methods to extract molecular and bulk chemical information from series
1042 of complex mass spectra with limited mass resolution, *Int. J. Mass Spectrom.*, 389, 26-38,
1043 <https://doi.org/10.1016/j.ijms.2015.08.011>, 2015.
- 1044
- 1045 Stockwell, C. E., Yokelson, R. J., Kreidenweis, S. M., Robinson, A. L., DeMott, P. J., Sullivan, R. C., Reardon, J., Ryan,
1046 K. C., Griffith, D. W. T., and Stevens, L.: Trace gas emissions from combustion of peat, crop residue, domestic biofuels,
1047 grasses, and other fuels: configuration and Fourier transform infrared (FTIR) component of the fourth Fire Lab at
1048 Missoula Experiment (FLAME-4), *Atmos. Chem. Phys.*, 14, 9727-9754, <https://doi.org/10.5194/acp-14-9727-2014>,
1049 2014.
- 1050
- 1051 Stockwell, C. E., Veres, P. R., Williams, J., and Yokelson, R. J.: Characterization of biomass burning emissions from
1052 cooking fires, peat, crop residue, and other fuels with high-resolution proton-transfer-reaction time-of-flight mass
1053 spectrometry, *Atmos. Chem. Phys.*, 15, 845-865, <https://doi.org/10.5194/acp-15-845-2015>, 2015.
- 1054
- 1055 Stockwell, C. E., Jayarathne, T., Cochrane, M. A., Ryan, K. C., Putra, E. I., Saharjo, B. H., Nurhayati, A. D., Albar, I.,
1056 Blake, D. R., Simpson, I. J., Stone, E. A., and Yokelson, R. J.: Field measurements of trace gases and aerosols emitted by
1057 peat fires in Central Kalimantan, Indonesia, during the 2015 El Niño, *Atmos. Chem. Phys.*, 16, 11711-11732,
1058 <https://doi.org/10.5194/acp-16-11711-2016>, 2016.
- 1059
- 1060 Stönnner, C., Derstroff, B., Klüpfel, T., Crowley, J. N., and Williams, J.: Glyoxal measurement with a proton transfer
1061 reaction time of flight mass spectrometer (PTR-TOF-MS): characterization and calibration. *J. Mass Spectrom.*, 52, 30-
1062 35. <https://doi.org/10.1002/jms.3893>, 2017.
- 1063



- 1064 Sudo, K. and Akimoto, H.: Global source attribution of tropospheric ozone: Long-range transport from various source
1065 regions, *J. Geophys. Res. Atmos.*, 112, <https://doi.org/10.1029/2006JD007992>, 2007.
1066
- 1067 Theys, N., Volkamer, R., Müller, J. F., Zarzana, K. J., Kille, N., Clarisse, L., De Smedt, I., Lerot, C., Finkenzeller, H.,
1068 Hendrick, F., Koenig, T. K., Lee, C. F., Knote, C., Yu, H., and Van Roozendael, M.: Global nitrous acid emissions and
1069 levels of regional oxidants enhanced by wildfires, *Nat. Geosci.*, 13, 681–686, <https://doi.org/10.1038/s41561-020-0637-7>,
1070 2020.
1071
- 1072 Tomsche, L., Piel, F., Mikoviny, T., Nielsen, C. J., Guo, H., Campuzano-Jost, P., Nault, B. A., Schueneman, M. K.,
1073 Jimenez, J. L., Halliday, H., Diskin, G., DiGangi, J. P., Nowak, J. B., Wiggins, E. B., Gargulinski, E., Soja, A. J., and
1074 Wisthaler, A.: Measurement report: Emission factors of NH₃ and NH_x for wildfires and agricultural fires in the United
1075 States, *Atmos. Chem. Phys.*, 23, 2331–2343, <https://doi.org/10.5194/acp-23-2331-2023>, 2023.
1076
- 1077 Thornhill, G. D., Ryder, C. L., Highwood, E. J., Shaffrey, L. C., and Johnson, B. T.: The effect of South American
1078 biomass burning aerosol emissions on the regional climate, *Atmos. Chem. Phys.*, 18, 5321–5342,
1079 <https://doi.org/10.5194/acp-18-5321-2018>, 2018.
1080
- 1081 Tian, H., Lu, C., Ciaia, P., Michalak, A. M., Canadell, J. G., Saikawa, E., Huntzinger, D. N., Gurney, K. R., Sitch, S.,
1082 Zhang, B., Yang, J., Bousquet, P., Bruhwiler, L., Chen, G., Dlugokencky, E., Friedlingstein, P., Melillo, J., Pan, S.,
1083 Poulter, B., Prinn, R., Saunio, M., Schwalm, C. R., and Wofsy, S. C.: The terrestrial biosphere as a net source of
1084 greenhouse gases to the atmosphere, *Nature*, 531, 225–228, <https://doi.org/10.1038/nature16946>, 2016.
1085
- 1086 Tsimpidi, A. P., Karydis, V. A., Pandis, S. N., and Lelieveld, J.: Global-scale combustion sources of organic aerosols:
1087 sensitivity to formation and removal mechanisms, *Atmos. Chem. Phys.*, 17, 7345–7364, <https://doi.org/10.5194/acp-17-7345-2017>, 2017.
1088
- 1089 Urbanski, S. P., Hao, W. M. and Baker, S.: Chapter 4 Chemical Composition of Wildland Fire Emissions, *Dev. Environ.*
1090 *Sci.*, 8, 79–107, [https://doi.org/10.1016/S1474-8177\(08\)00004-1](https://doi.org/10.1016/S1474-8177(08)00004-1), 2008.
1091
- 1092 Vasilkov, A., Krotkov, N., Yang, E. S., Lamsal, L., Joiner, J., Castellanos, P., Fasnacht, Z., and Spurr, R.: Explicit and
1093 consistent aerosol correction for visible wavelength satellite cloud and nitrogen dioxide retrievals based on optical
1094 properties from a global aerosol analysis, *Atmos. Meas. Tech.*, 14, 2857–2871, <https://doi.org/10.5194/amt-14-2857-2021>, 2021.
1095
- 1096 Vay, S. A., Tyler, S. C., Choi, Y., Blake, D. R., Blake, N. J., Sachse, G. W., Diskin, G. S., and Singh, H. B.: Sources and
1097 transport of $\Delta^{14}\text{C}$ in CO₂ within the Mexico City Basin and vicinity, *Atmos. Chem. Phys.*, 9, 4973–4985,
1098 <https://doi.org/10.5194/acp-9-4973-2009>, 2009.
1099
- 1100 Veres, P. R., Neuman, J. A., Bertram, T. H., Assaf, E., Wolfe, G. M., Williamson, C. J., Weinzierl, B., Tilmes, S.,
1101 Thompson, C. R., Thames, A. B., Schroder, J. C., Saiz-Lopez, A., Rollins, A. W., Roberts, J. M., Price, D., Peischl, J.,
1102 Nault, B. A., Møller, K. H., Müller, D. O., Meinardi, S., Li, Q., Lamarque, J.-F., Kupc, A., Kjaergaard, H. G., Kinnison,
1103 D., Jimenez, J. L., Jernigan, C. M., Hornbrook, R. S., Hills, A., Dollner, M., Day, D. A., Cuevas, C. A., Campuzano-Jost,
1104 P., Burkholder, J., Bui, T. P., Brune, W. H., Brown, S. S., Brock, C. A., Bourgeois, I., Blake, D. R., Apel, E. C., and
1105 Ryerson, T. B.: Global airborne sampling reveals a previously unobserved dimethyl sulfide oxidation mechanism in the
1106 marine atmosphere, *P. Natl. Acad. Sci.*, 117, 4505, <https://doi.org/10.1073/pnas.1919344117>, 2020.
1107
- 1108 Wang, S., Coggon, M. M., Gkatzelis, G. I., Warneke, C., Bourgeois, I., Ryerson, T. B., Peischl, J., Veres, P. R., Neuman,
1109 J. A., Hair, J., Shingler, T., Fenn, M., Diskin, G., Huey, L. G., Lee, Y. R., Apel, E. C., Hornbrook, R. S., Hills, A. J.,
1110 Hall, S. R., Ullmann, K., Bela, M. M., Trainer, M. K., Kumar, R., Orlando, J. J., Flocke, F. M., and Emmons, L. K.:
1111 Chemical Tomography in a Fresh Wildland Fire Plume: a Large Eddy Simulation (LES) Study, *J. Geophys. Res. Atmos.*,
1112 126, e2021JD035203, <https://doi.org/10.1029/2021JD035203>, 2021.
1113
- 1114 Ward, D. S., Kloster, S., Mahowald, N. M., Rogers, B. M., Randerson, J. T., and Hess, P. G.: The changing radiative
1115 forcing of fires: global model estimates for past, present and future, *Atmos. Chem. Phys.*, 12, 10857–10886,
1116 <https://doi.org/10.5194/acp-12-10857-2012>, 2012.
1117
- 1118 Warneke, C., Roberts, J. M., Veres, P., Gilman, J., Kuster, W. C., Burling, I., Yokelson, R., and de Gouw, J. A.: VOC
1119 identification and inter-comparison from laboratory biomass burning using PTR-MS and PIT-MS, *Int. J. Mass*
1120 *Spectrom.*, 303, 6–14, <https://doi.org/10.1016/j.ijms.2010.12.002>, 2011.
1121
- 1122
1123



- 1124 Weibring, P., Richter, D., Walega, J. G., and Fried, A.: First demonstration of a high performance difference frequency
1125 spectrometer on airborne platforms, *Opt. Express*, 15, 13476-13495, <https://doi.org/10.1364/OE.15.013476>, 2007.
1126
- 1127 Westerling, A. L., Hidalgo, H. G., Cayan, D. R., and Swetnam, T. W.: Warming and Earlier Spring Increase Western
1128 U.S. Forest Wildfire Activity, *Science*, 313, 940, <https://doi.org/10.1126/science.1128834>, 2006.
1129
- 1130 Wiedinmyer, C. and Hurteau, M. D.: Prescribed Fire As a Means of Reducing Forest Carbon Emissions in the Western
1131 United States, *Environ. Sci. Technol.*, 44, 1926-1932, <https://doi.org/10.1021/es902455e>, 2010.
1132
- 1133 Wiedinmyer, C., Akagi, S. K., Yokelson, R. J., Emmons, L. K., Al-Saadi, J. A., Orlando, J. J., and Soja, A. J.: The Fire
1134 Inventory from NCAR (FINN): a high resolution global model to estimate the emissions from open burning, *Geosci.
1135 Model Dev.*, 4, 625-641, <https://doi.org/10.5194/gmd-4-625-2011>, 2011.
1136
- 1137 Wiggins, E. B., Soja, A. J., Gargulinski, E., Halliday, H. S., Pierce, R. B., Schmidt, C. C., Nowak, J. B., DiGangi, J. P.,
1138 Diskin, G. S., Katich, J. M., Perring, A. E., Schwarz, J. P., Anderson, B. E., Chen, G., Crosbie, E. C., Jordan, C.,
1139 Robinson, C. E., Sanchez, K. J., Shingler, T. J., Shook, M., Thornhill, K. L., Winstead, E. L., Ziemba, L. D., and Moore,
1140 R. H.: High Temporal Resolution Satellite Observations of Fire Radiative Power Reveal Link Between Fire Behavior
1141 and Aerosol and Gas Emissions, *Geophys. Res. Lett.*, 47, e2020GL090707, <https://doi.org/10.1029/2020GL090707>,
1142 2020.
1143
- 1144 Wolfe, G. M., Hanisco, T. F., Arkinson, H. L., Blake, D. R., Wisthaler, A., Mikoviny, T., Ryerson, T. B., Pollack, I.,
1145 Peischl, J., Wennberg, P. O., Crounse, J. D., St. Clair, J. M., Teng, A., Huey, L. G., Liu, X., Fried, A., Weibring, P.,
1146 Richter, D., Walega, J., Hall, S. R., Ullmann, K., Jimenez, J. L., Campuzano-Jost, P., Bui, T. P., Diskin, G., Podolske, J.
1147 R., Sachse, G., and Cohen, R. C.: Photochemical evolution of the 2013 California Rim Fire: synergistic impacts of
1148 reactive hydrocarbons and enhanced oxidants, *Atmos. Chem. Phys.*, 22, 4253-4275, [https://doi.org/10.5194/acp-22-
1149 4253-2022](https://doi.org/10.5194/acp-22-4253-2022), 2022.
1150
- 1151 Xu, L., Crounse John, D., Vasquez Krystal, T., Allen, H., Wennberg Paul, O., Bourgeois, I., Brown Steven, S.,
1152 Campuzano-Jost, P., Coggon Matthew, M., Crawford James, H., DiGangi Joshua, P., Diskin Glenn, S., Fried, A.,
1153 Gargulinski Emily, M., Gilman Jessica, B., Gkatzelis Georgios, I., Guo, H., Hair Johnathan, W., Hall Samuel, R.,
1154 Halliday Hannah, A., Hanisco Thomas, F., Hannun Reem, A., Holmes Christopher, D., Huey, L. G., Jimenez Jose, L.,
1155 Lamplugh, A., Lee Young, R., Liao, J., Lindaas, J., Neuman, J. A., Nowak John, B., Peischl, J., Peterson David, A., Piel,
1156 F., Richter, D., Rickly Pamela, S., Robinson Michael, A., Rollins Andrew, W., Ryerson Thomas, B., Sekimoto, K.,
1157 Selimovic, V., Shingler, T., Soja Amber, J., St. Clair Jason, M., Tanner David, J., Ullmann, K., Veres Patrick, R.,
1158 Walega, J., Warneke, C., Washenfelder Rebecca, A., Weibring, P., Wisthaler, A., Wolfe Glenn, M., Womack Caroline,
1159 C., and Yokelson Robert, J.: Ozone chemistry in western U.S. wildfire plumes, *Sci. Adv.*, 7, eabl3648,
1160 <https://doi.org/10.1126/sciadv.abl3648>, 2021.
1161
- 1162 van der Velde, I. R., van der Werf, G. R., Houweling, S., Eskes, H. J., Veeffkind, J. P., Borsdorff, T., and Aben, I.:
1163 Biomass burning combustion efficiency observed from space using measurements of CO and NO₂ by the
1164 TROPOspheric Monitoring Instrument (TROPOMI), *Atmos. Chem. Phys.*, 21, 597-616, [https://doi.org/10.5194/acp-21-
1165 597-2021](https://doi.org/10.5194/acp-21-597-2021), 2021.
1166
- 1167 Yokelson, R. J., Griffith, D. W. T., and Ward, D. E.: Open-path Fourier transform infrared studies of large-scale
1168 laboratory biomass fires, *J. Geophys. Res. Atmos.*, 101, 21067-21080, <https://doi.org/10.1029/96JD01800>, 1996.
1169
- 1170 Yokelson, R. J., Christian, T. J., Karl, T. G., and Guenther, A.: The tropical forest and fire emissions experiment:
1171 laboratory fire measurements and synthesis of campaign data, *Atmos. Chem. Phys.*, 8, 3509-3527,
1172 <https://doi.org/10.5194/acp-8-3509-2008>, 2008.
1173
- 1174 Yokelson, R. J., Burling, I. R., Gilman, J. B., Warneke, C., Stockwell, C. E., de Gouw, J., Akagi, S. K., Urbanski, S. P.,
1175 Veres, P., Roberts, J. M., Kuster, W. C., Reardon, J., Griffith, D. W. T., Johnson, T. J., Hosseini, S., Miller, J. W.,
1176 Cocker Iii, D. R., Jung, H., and Weise, D. R.: Coupling field and laboratory measurements to estimate the emission
1177 factors of identified and unidentified trace gases for prescribed fires, *Atmos. Chem. Phys.*, 13, 89-116,
1178 <https://doi.org/10.5194/acp-13-89-2013>, 2013.
1179
- 1180 Yuan, B., Koss, A., Warneke, C., Gilman, J. B., Lerner, B. M., Stark, H., and de Gouw, J. A.: A high-resolution time-of-
1181 flight chemical ionization mass spectrometer utilizing hydronium ions (H₃O⁺ ToF-CIMS) for measurements of volatile
1182 organic compounds in the atmosphere, *Atmos. Meas. Tech.*, 9, 2735-2752, <https://doi.org/10.5194/amt-9-2735-2016>,
1183 2016.
1184



- 1185 Yue, C., Ciais, P., Cadule, P., Thonicke, K., and van Leeuwen, T. T.: Modelling the role of fires in the terrestrial carbon
1186 balance by incorporating SPITFIRE into the global vegetation model ORCHIDEE – Part 2: Carbon emissions and the
1187 role of fires in the global carbon balance, *Geosci. Model Dev.*, 8, 1321-1338, <https://doi.org/10.5194/gmd-8-1321-2015>,
1188 2015.
- 1189
1190 Zarzana, K. J., Selimovic, V., Koss, A. R., Sekimoto, K., Coggon, M. M., Yuan, B., Dubé, W. P., Yokelson, R. J.,
1191 Warneke, C., de Gouw, J. A., Roberts, J. M., and Brown, S. S.: Primary emissions of glyoxal and methylglyoxal from
1192 laboratory measurements of open biomass burning, *Atmos. Chem. Phys.*, 18, 15451-15470, [https://doi.org/10.5194/acp-](https://doi.org/10.5194/acp-18-15451-2018)
1193 [18-15451-2018](https://doi.org/10.5194/acp-18-15451-2018), 2018.
- 1194
1195 Zhao, X. and Wang, L.: Atmospheric Oxidation Mechanism of Furfural Initiated by Hydroxyl Radicals, *The Journal of*
1196 *Physical Chemistry A*, 121, 3247-3253, <https://doi.org/10.1021/acs.jpca.7b00506>, 2017.
- 1197
1198 Zheng, W., Flocke, F. M., Tyndall, G. S., Swanson, A., Orlando, J. J., Roberts, J. M., Huey, L. G., and Tanner, D. J.:
1199 Characterization of a thermal decomposition chemical ionization mass spectrometer for the measurement of peroxy acyl
1200 nitrates (PANs) in the atmosphere, *Atmos. Chem. Phys.*, 11, 6529-6547, <https://doi.org/10.5194/acp-11-6529-2011>,
1201 2011.